Jet Substructure at the Tevatron and LHC: New results, new tools, new benchmarks∗

A Altheimer[1], S Arora[2], L Asquith[3], G Brooijmans[1], J Butterworth[4], M Campanelli[4], B Chapleau[5], A E Cholakian[1,6], J P Chou[7], M Dasgupta[8], A Davison[4], J Dolen[9], S D Ellis[10], R Essig[11,12,13], J J Fan[14], R Field[15], A Fregoso[8], J Gallicchio[6], Y Gershtein[2], A Gomes[16], A Haas[11], E Halkiadakis[2], V Halyo[14], S Hoeche[11], A Hook[11,17], A Hornig[10], P Huang[18], E Izaguirre[11,17], M Jankowiak[11,17], G Kribs[19,20], D Krohn[6], A J Larkoski[11], A Lath[2], C Lee[21], S J Lee[22], P Loch[23], P Maksimovic[24], M Martinez[25], D W Miller[11,17], T Plehn[26], K Prokofiev[27], R Rahmat[28], S Rappoccio[24], A Safonov[29], G P Salam[30,14,31], S Schumann[32], M D Schwartz[6], A Schwartzman[11], M Seymour[8], J Shao[33], P Sinervo[34], M Son[35], D E Soper[20], M Spannowsky[36], I W Stewart[21], M Strassler[2], E Strauss[11], M Takeuchi[26], J Thaler[21], S Thomas[2], B Tweedie[37], R Vasquez Sierra[9], C K Vermilion[38,39], M Villaplana[40], M Vos[40], J Wacker[11], D Walker[6], J R Walsh[38,41], L-T Wang[14], S Wilbur[42] and W Zhu[14]

[1] Columbia University, Nevis Laboratory, 136 S Broadway, Irvington, NY 10533, USA
[2] Rutgers University, Department of Physics and Astronomy, 136 Frelinghuysen Road, Piscataway, NJ 08854, USA
[3] Argonne National Laboratory, 9700 S. Cass Avenue Argonne, IL 60439, USA
[4] Department of Physics and Astronomy, University College London, WC1E 6BT, UK
[5] McGill University, High Energy Physics Group, 3600 University Street, Montréal, Québec H3A 2T8, Canada
[6] Department of Physics, Harvard University, Cambridge, MA 02138, USA
[7] Department of Physics, Brown University, Box 1843, Providence, RI 02912, USA
[8] School of Physics and Astronomy, University of Manchester, Manchester, M13 9PL, UK
[9] University of California, Davis, Davis, CA 95616, USA
[10] Department of Physics, University of Washington, Box 351560, Seattle, WA 98195, USA
[11] SLAC National Accelerator Laboratory, Menlo Park, CA 94025, USA
[12] C.N. Yang Institute for Theoretical Physics, Stony Brook University, Stony Brook, NY 11794, USA

[13] School of Natural Sciences, Institute for Advanced Study, Einstein Drive, Princeton, NJ 08544, USA

[14] Department of Physics, Princeton University, Princeton, NJ 08544, USA

[15] Department of Physics, University of Florida, Gainesville, FL 32611, USA

[16] Laboratório de Instrumentaçao e Física Experimental de Partículas, 1000-149 Lisboa, Portugal

[17] Department of Physics, Stanford University, 382 Via Pueblo Mall, Stanford, CA 94305, USA

[18] Department of Physics, University of Wisconsin–Madison, 1150 University Ave, Madison, WI 53706, USA

[19] Fermi National Accelerator Laboratory, Batavia, IL, 60510, USA

[20] Institute of Theoretical Science, University of Oregon, Eugene, OR 97403, USA

[21] Center for Theoretical Physics, Massachusetts Institute of Technology, Cambridge, MA 02139

[22] Department of Physics, KAIST, Daejeon 305-701, Korea

[23] Department of Physics, University of Arizona, Tucson, AZ 85719, USA

[24] Department of Physics and Astronomy, Johns Hopkins University, 3400 N. Charles St., Baltimore, MD 21218, USA

[25] ICREA and Institut de Fsica d'Altes Energies, UAB Campus Bellaterra, 08193 Barcelona, Spain

[26] Institute for Theoretical Physics, Uni Heidelberg, Philosophenweg 16, D-69120 Heidelberg, Germany

[27] Department of Physics, New York University, 4 Washington Pl, New York, NY 10003, USA

[28] Department of Physics and Astronomy, The University of Mississippi, University, MS 38677, USA

[29] Department of Physics and Astronomy, Texas A&M University, 4242 TAMU, College Station, TX 77843, USA

[30] Department of Physics, Theory Unit, CERN, CH-1211 Geneva 23, Switzerland

[31] LPTHE, UPMC Univ. Paris 6 and CNRS UMR 7589, Paris, France

[32] II. Physikalisches Institut, Universität Göttingen, 37077 Göttingen, Germany

[33] Department of Physics, Syracuse University, Syracuse, NY 13244, USA

[34] Department of Physics, University of Toronto, 60 Saint George Street, Toronto, M5S 1A7, Ontario, Canada

[35] Department of Physics, Yale University, New Haven, CT 06511, USA

[36] IPPP, Department of Physics, Durham University, UK

[37] Physics Department, Boston University, Boston, MA 02215, USA

[38] Ernest Orlando Lawrence Berkeley National Laboratory, University of California, Berkeley, CA 94720

[39] Department of Physics & Astronomy, University of Louisville, Louisville, KY 40292, USA

[40] Instituto de Física Corpuscular, IFIC/CSIC-UVEG, PO Box 22085, 46071 Valencia, Spain

[41] Center for Theoretical Physics, University of California, Berkeley, CA 94720, USA

[42] Department of Physics, University of Chicago, 5720 S Ellis Ave, Chicago, IL 60637, USA

Abstract. In this report we review recent theoretical progress and the latest experimental results in jet substructure from the Tevatron and the LHC. We review the status of and outlook for calculation and simulation tools for studying jet substructure. Following up on the report of the Boost 2010 workshop, we present a new set of benchmark comparisons of substructure techniques, focusing on the set of variables and grooming methods that are collectively known as "top taggers". To facilitate further exploration, we have attempted to collect, harmonise, and publish software implementations of these techniques.

1. Introduction

At the time of the first BOOST meeting, at SLAC in July 2009, several groups had begun to argue that jet substructure — the internal characteristics of hadronic jets — could be useful in identifying the decays of heavy particles at the Large Hadron Collider. By the following year, a trickle had become a flood. Some techniques had received detailed attention from experimental groups, and the increasing quantity of data available meant that background studies were beginning to be possible. Another year has passed, and the stream of theoretical advances shows no signs of abating. Many new substructure measurements and techniques have been proposed, and significant progress has been made in developing the theoretical tools to calculate distributions in substructure observables. Meanwhile, sufficient data now exist to study the boosted hadronic decays of heavy Standard Model particles such as the W boson and top quark.

This report, an outgrowth of the BOOST 2011 workshop held at Princeton University in May 2011, aims to summarise recent theoretical and experimental progress, outline goals for the near future, and provide benchmark comparisons and tools to help achieve these goals.

In Section 2, we review recent substructure results at the Tevatron and LHC. In Section 3, we survey new proposals for substructure techniques. In Section 4, we describe the new software tools for studying jet substructure in FastJet 3. In Section 5, we extend the benchmark top-tagging comparisons found in last year's report [1] with new methods, new Monte Carlo samples, and detector simulation. The samples, as well as software to implement the techniques compared and our detector model, are publicly available, either as part of the FastJet 3.0.0 package or as FastJet-based tools. Finally, in Section 6, we survey the status of substructure predictions and discuss goals for new calculations and measurements in the coming year.

2. New results from the Tevatron and LHC

Several recent experimental results from the Fermilab Tevatron were presented at the BOOST 2011 workshop, exploring different aspects of boosted physics. These could be categorised into two broad classes: studies that elucidate the behaviour of Standard Model physics processes when subjected to various degrees of boost, and searches for

new physics using boosted object signatures. All the analyses were performed on samples of $\sqrt{s} = 1.96$ TeV proton-antiproton collisions produced over the last eight years at the Tevatron. Results from the Tevatron's two detectors are presented here in Section 2.1 for CDF and Section 2.2 for D0.

The LHC started colliding protons at a center of mass energy $\sqrt{s} = 7$ TeV on March 30, 2010. Just over 18 months and 5 fb^{-1} later, the ATLAS and CMS experiments have collected sufficient data to have a realistic chance of using substructure techniques to uncover massive boosted particles such as W/Z bosons, top quarks, and whatever else may lie in wait. The experimental results presented in these proceedings focus on the results made public prior to the BOOST workshop in May 2011. For both ATLAS and CMS this means two analyses: a paper from each on jet shapes [2], [3] and a conference note on jet substructure [4], [5].

The most important and interesting results of these studies are summarised in Section 2.3 for ATLAS and Section 2.4 for CMS. Sensitivities to pile-up and detector effects, seen by the experimental community as the most pressing issues in jet and jet substructure studies, feature prominently.

All of these experiments must in varying degrees grapple with the presence of multiple simultaneous proton-(anti-)proton interactions, or pile-up, within every bunch crossing. These additional collisions are uncorrelated with the hard-scattering process that triggers the event and create a background of soft diffuse radiation that offsets the energy measurement of jets and impacts jet shape and substructure measurements. It is essential that measurements of jet substructure be able to disentangle or correct for the influence of pile-up.

Observables designed to be sensitive to the internal structure of jets are expected to also be sensitive to pile-up [1]. Large-radius jets, such as those used in the measurements of jet substructure, are naturally more susceptible to pile-up due to their larger catchment area [6]; the invariant mass of these large jets is particularly affected [7]. Techniques for correcting for these effects — as in the CDF analyses — or mitigating their impact — such as the splitting and filtering procedure pioneered in ATLAS — are essential in producing precision measurements for several of the analyses presented by the Tevatron and LHC experiments. A more thorough review of these issues at ATLAS can be found in [8].

2.1. Results from CDF

2.1.1. Pile-up at CDF In the context of measurements of the mass, angularity and planar flow of high-p_T jets [9], a new method of correcting the jet mass for pile-up was developed. The use of a complementary cone at right angles to the jet in azimuthal angle ϕ and at approximately the same pseudorapidity allows the energy density from both underlying event (UE) and multiple interactions (MI) to be measured. The underlying event refers to the interactions and hadronisation of partons in the colliding protons other than the partons in the hard process. Multiple interactions refer to both "in-time"
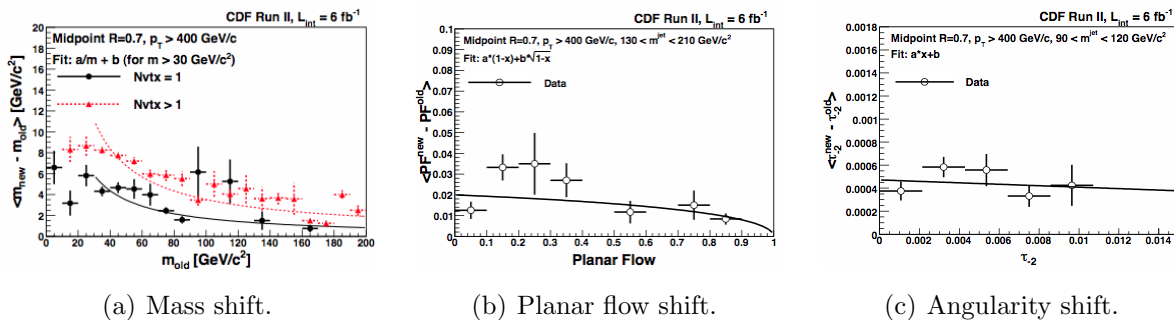
(a) Mass shift. (b) Planar flow shift. (c) Angularity shift.

Figure 1. The correction to the jet mass (a) from additional energy deposition due to MI+UE (Nvtx > 1 events) compared with the jet mass corrections for UE alone (Nvtx = 1 events) for jets with a cone size of $R = 0.7$. The estimated shift from the combination of UE and MI in planar flow (b) and angularity (c) as measured in data. The average number of collisions per bunch crossing is $\sim$ 3 for this data sample.

and "out-of-time" pile-up: the former describing multiple proton-proton collisions in a single bunch crossing, the latter describing the delayed instrumental effects of previous crossings. The incoherent contributions to the shift in jet mass from MI were isolated from the partially coherent contributions due to UE by examining the mass shift as a function of the number of good vertices in the event. The average shift in the jet mass when adding the towers from the complementary cone into the jet are shown in Figure 1 along with the MI+UE corrections measured for angularity and planar flow. The high mass selections made as part of the angularity and planar flow measurements resulted in too few events to separate the UE (single-vertex) and MI (single- and multiple-vertex) components.

2.1.2. New physics searches in multijet events at CDF The results of a search for pair production of a supersymmetric particle that decays strongly and violates R-parity were described in [10]. The final state of interest was at least six quarks, most observed as separate jets, and no missing transverse energy in the event. The challenge for this search was to reduce the large backgrounds from QCD multijet production, which was done by placing specific kinematic requirements on three-jet triplets in the final state.

The analysis sought events in a CDF sample that satisfied a trigger requiring at least four jets with $p_T > 15$ GeV and the sum of the calorimeter transverse energy greater than 175 GeV. Events were furthermore required to have at least six jets with $p_T > 15$ GeV and $|\eta| < 2.5$, and the scalar sum of the six highest-energy jets was required to be greater than 250 GeV. The missing transverse energy, $\not{E}_T$, was required to be less than 50 GeV in order to reduce contributions from W boson final states and mis-measured QCD events.

All twenty combinations (or more) of three-jet triplets that could be produced from jets with $p_T > 15$ GeV were considered and the invariant mass of each combination, M_{jjj},

and the sum of the magnitudes of the transverse momenta of the three jets, $\sum_{jjj}|p_T|$, were formed. Monte Carlo studies have shown that requiring

$$\sum_{jjj}|p_T| - M_{jjj} > \Delta \tag{1}$$

is an efficient way of separating potential signal combinations (where M_{jjj} would be a constant reflecting the mass of the supersymmetric parent) from the QCD and combinatorial backgrounds. Δ is a constant optimized for each assumed parent mass. This is in effect a boosted three-jet final state. The shape of the backgrounds in M_{jjj} were estimated by using a five-jet final state, showing that the background is expected to peak around 100 GeV.

The M_{jjj} distribution was then fit to a combination of signal and background terms, where the signal was defined by a PYTHIA Monte Carlo calculation for R-parity violating (RPV) gluino pair production. Although the acceptance for the gluino final state is quite low (roughly 5×10^{-5}), CDF was able to set significant limits on the RPV gluino cross section, which were then converted into lower limits on the gluino mass. Lower mass limits ranging from 144 to 154 GeV at 95% C.L. were set on the gluino mass, depending on the assumptions about the spectrum of intermediate supersymmetric final states. What is perhaps as interesting is that CDF observed evidence for a boosted top quark signature. In the top quark mass region of $M_{jjj} \sim 175$ GeV, CDF observed 11 ± 5 jet triplets. Although one expects on average only one top quark event in this kinematic region, the shape of the mass distribution is consistent with what one expects from MC simulations.

2.1.3. Boosted top quark search at CDF CDF presented updated results on the measurements of jet mass, angularity and planar flow for jets with $p_T > 400$ GeV from a sample of 5.95 fb^{-1} [11]. The measured distributions were compared with analytical expressions from NLO QCD calculations, as well as PYTHIA 6.1.4 predictions incorporating full detector simulation. The theory predictions for jet mass were in good agreement with the data, whereas the angularity and planar flow predictions by PYTHIA showed disagreement in detail (primarily at low angularity and low planar flow).

CDF used these data to also search for a signal of boosted top quark production. Candidate events were selected in two channels: the fully hadronic decays where both top quarks produce massive high-p_T jets (the "1+1" channel), and the decays where one top quark decays semi-leptonically resulting in one massive high-p_T jet recoiling against a second lower-mass jet and significant missing transverse energy (the "SL" final state). A signal region in the 1+1 mode was defined by requiring both leading jets to have a mass between 130 and 210 GeV (see Figure 2), while the signal region in the SL mode requires the leading jet to have $130 < m^{\text{jet1}} < 210$ GeV and the event to have missing transverse energy significance

$$S_{MET} \equiv \not{E}_T / \sqrt{\sum E_T} \in (4, 10). \tag{2}$$

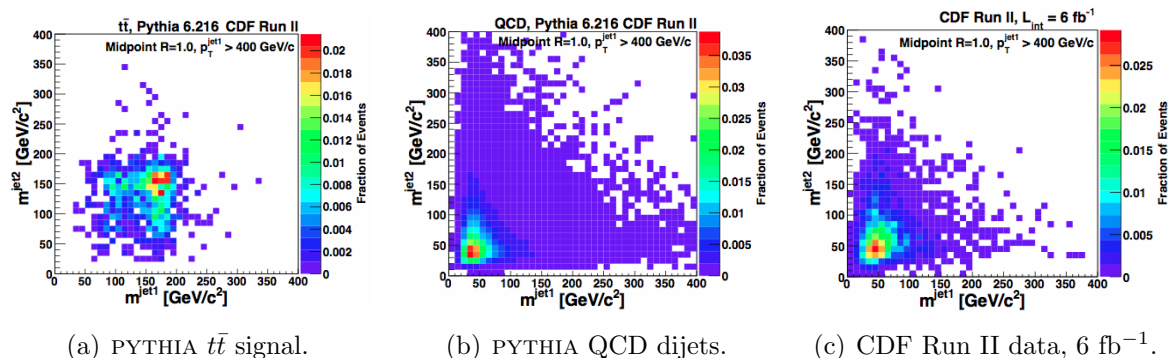(a) PYTHIA $t\bar{t}$ signal.   (b) PYTHIA QCD dijets.   (c) CDF Run II data, 6 fb^{-1}.

Figure 2. The m^{jet2} versus m^{jet1} distribution for all events with at least one jet with $p_T > 400$ GeV and $\eta < 0.7$, using $R = 1.0$ Midpoint cones. MI corrections have been performed and all events are required to have $S_{MET} < 4$.

This cut rejects primarily QCD dijet events. The remaining QCD backgrounds are estimated by looking at the event rates in sideband regions of jet mass and S_{MET}. The analysis observes 31 and 26 candidate events in the 1+1 and SL channels, respectively, and the backgrounds are estimated to be 14.6 ± 2.7 and 31.3 ± 8.1 events, respectively. The total number of top quark events expected in the two channels is 4.9 ± 2.1 candidates.

Although the data are consistent with a boosted top quark signature, they are not statistically strong enough to claim observation. Rather, they are used to set an upper limit of 38 fb on top quarks produced with $p_T > 400$ GeV. The SM expectation for this cross section is 4.5 fb.

2.1.4. Search for lepton jets at CDF There are several theories beyond the Standard Model that predict the production of cascades of particles that appear in the final state as a "lepton jet". The CDF collaboration reported on a search for such objects using 5.1 fb^{-1} of $\sqrt{s} = 1.96$ TeV proton-antiproton collisions at the Tevatron. The search looked for events with a large number of low-energy leptons produced in association with a W or Z boson.

Events were selected by performing the standard selection for W or Z boson candidates, requiring at least one well-identified electron or muon candidate and then either significant $\not{E}_T$ or a second well-identified charged lepton of the same flavour but opposite charge. A "soft lepton" algorithm was then employed to identify additional electron or muon candidates down to a transverse momentum of 1 GeV for electrons and 3 GeV for muons. The numbers of events in the zero or one additional lepton bins were used to scale the expected backgrounds for the signal region defined by two or more soft lepton candidates. The analysis found that the dominant backgrounds came from inclusive W+jets production where one or more of the jets were mis-identified, or Drell-Yan production where the additional leptons were mis-identified jets. Other sources of background, such was W+c-quark, W+b-quark, $t\bar{t}$ and di-vector boson production were also evaluated.

The potential signal was modelled on a benchmark process defined by a neutralino model with a "hidden" Higgs boson coupled to a dark sector, where the dark sector particles decay to pairs of charged leptons [12]. The channels with the best signal-to-background for this model were those with a W or Z boson with at least three additional muons, either with none or one additional electron; for example, in the channel with a $W+3$ additional muons, one expected 1.5 ± 1.2 background events and nine signal events (only two events were observed). There was no signal observed above background, and a 95% C.L. upper limit on the production cross section of a W or Z boson produced in association with a Higgs boson with the expected couplings of 27 fb was set. This allowed the collaboration to rule out the benchmark model.

This analysis showed the effectiveness of using the lepton jet signatures to search for evidence of new physics.

2.2. Results from D0

2.2.1.   Colour Flow in D0 $t\bar{t}$ Events The D0 experiment presented recent results showing how the colour flow that is expected to arise between two jets can be used as a discriminant to identify W boson hadronic decays in a 5.3 fb^{-1} sample of $t\bar{t}$ events [13]. Since the W decay products form a colour singlet, they produce an antenna radiation pattern, with most soft particles emitted between the two jet directions. The "pull" of the jets' radiation toward each other can be used to more effectively identify dijet systems arising from a specific colour state.

Events were selected by requiring the traditional lepton+jets final state, with a charged lepton, missing transverse energy and four or more jets. At least two of the jets had to be tagged as b-quark candidates, resulting in 728 candidate events with an estimated background rate of 82 ± 9 events in the sample not arising from $t\bar{t}$ production. The jet pairs that had an invariant mass within 30 GeV of the W boson mass were then selected and the shape of the energy depositions studied to look for a signal consistent with the colour singlet. The minimum relative pull angle for jet pairs satisfying $|m_W - m_{j1j2}| < 30$ GeV, $\Delta R_{j1,j2} < 2$ and $|\eta| < 1$ is shown in Figure 3(a). The expected colour effect in the relative orientations of the jet pulls was observed when comparing the daughter jets from W boson decays and the b-quark jets, though the statistical power of the measurement was modest and the kinematics of the pairs of jets were not identical. A more direct comparison was made by producing Monte Carlo $t\bar{t}$ decays with a W boson produced as a colour octet compared with the expected colour singlet state, and a series of detailed studies were performed to evaluate the systematic uncertainties on this measurement.

The actual quantity measured was the fraction of singlet W boson decays compared with the total number, giving

$$f_{\text{singlet}} = 0.65^{+0.37}_{-0.38}\,(\text{stat.}) \pm 0.22\,(\text{syst.}). \tag{3}$$

This could be turned into a lower limit on the fraction of singlet decays of $f_{\text{singlet}} > 0.277$ at 95% C.L. Although this is somewhat higher than the limit that might have been
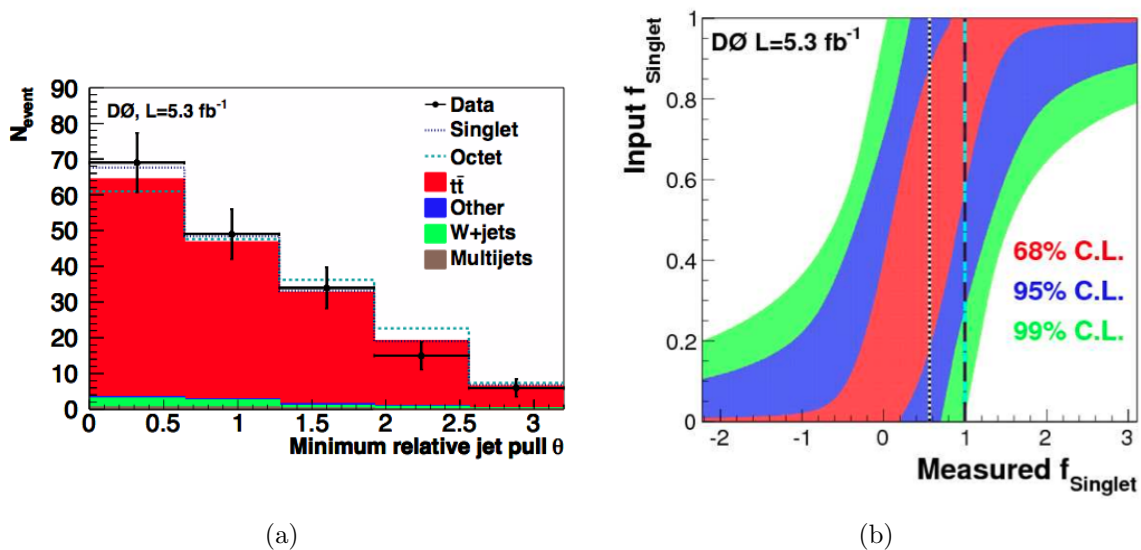
(a)   (b)

Figure 3. The minimum relative pull angle for W jets (a) is measured for jets satisfying $|m_W - m_{j1j2}| < 30$ GeV, $\Delta R_{j1,j2} < 2$ and $|\eta| < 1$. The expected C.L. bands for f_{singlet} are shown in (b); the dashed line shows the expected value and the dotted line indicates the measured value of f_{singlet}.

expected given the data sample, it is consistent with the expectation within statistical uncertainties. The expected C.L. bands for this limit are shown in Figure 3(b).

This means of measuring the colour flow provides an additional discriminant that can be used to search for decays of other boosted objects (such as $H \to b\bar{b}$) and gives us confidence that the modelling of colour flow is being done well in current Monte Carlo calculations.

2.3. Results from ATLAS

2.3.1. ATLAS and pile-up In the recent ATLAS analysis of 35 pb^{-1} of data [4] , the sensitivity of the individual jet mass to pile-up is directly tested. The increase in the mean jet mass as a function of the number of reconstructed good vertices (good vertices being defined as those with at least 5 tracks with $p_T > 150$ MeV), N_{PV}, is measured for jets with a p_T of at least 300 GeV and rapidity $|y| < 2$. The results are shown in Figure 4 for jets of various radii and built using two different jet algorithms. The mean jet mass is observed to increase linearly with N_{PV}. For events with only a single primary vertex, the mean jet mass increases linearly with R. The slope of the mean jet mass as a function of the number of primary vertices, though, exhibits a dependence on R that is consistent with the ratio of the third power of the jet resolution parameter. This follows the prediction of pQCD calculations [14]: the extra mass from an additional particle k scales like $\delta m^2 \approx 2p_T \cdot k \sim p_T p_T^k \Delta R_k^2$, so the net change from a uniform pile-up p_T density ρ is $\delta m^2 \sim p_T \rho \int dA \Delta R^2 \sim p_T \rho R^4$, and hence $\delta m \sim R^4 \rho p_T / m$. Since $m \sim R$, the derivative $dm/d\rho$ then scales like R^3 for fixed p_T.
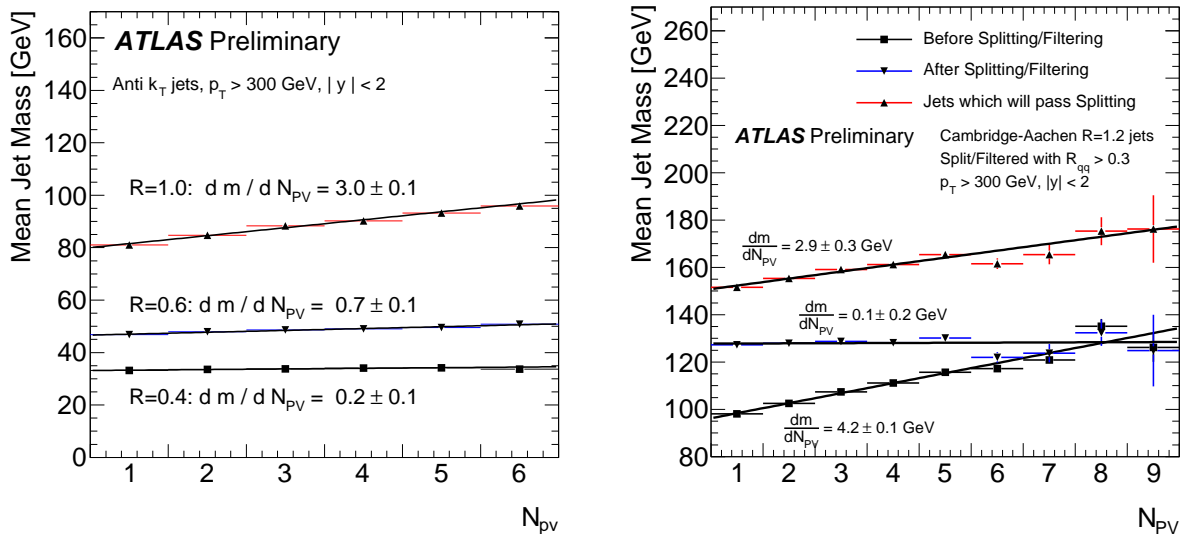
(a) Effect from jet area.

(b) Effect from filtering.

Figure 4. The mean mass for jets with $p_T > 300$ GeV as a function of the number of primary vertices identified in the event. Comparisons show the effect for (a) anti-k_T jets with different resolution parameters and (b) Cambridge-Aachen $R = 1.2$ jets with and without a splitting and filtering procedure. Each set of points is fitted with a straight line.

Figure 4 also shows the impact of pile-up on each of the three jet algorithms used in the ATLAS study. Specifically, Figure 4(b) shows the dependence on N_{PV} for the mean jet mass before and after the splitting and filtering procedure. The filtering procedure significantly reduces the effect of pile-up on jet mass. In fact, the slope of a straight line fit is consistent with zero. This result demonstrates that certain well-designed jet grooming procedures can significantly reduce the impact of pile-up and that the efficacy of the method can be tested *in-situ*. Methods to correct for these effects and to provide more general pile-up mitigation procedures using jet grooming are underway in ATLAS.

2.3.2. Jet shapes with ATLAS The study of jet shapes in proton-proton collisions provides information about the details of the parton-to-jet fragmentation process [15]. The internal structure of sufficiently energetic jets is primarily dictated by the emission of multiple gluons from the primary parton, calculable in perturbative QCD (pQCD). The shape of the jet depends on the type of parton (quark or gluon) and is also sensitive to non-perturbative fragmentation effects and underlying event (UE) contributions from the interaction between proton remnants. A proper modelling of the soft contributions is crucial for the understanding of jet production in hadron-hadron collisions and for comparison of the jet cross section measurements with pQCD theoretical predictions.

The ATLAS collaboration recently published results on differential and integrated jet shapes for jets constructed with the anti-k_T algorithm [16] with distance parameter

$R = 0.6$ [2]. The jet shapes were calculated using the constituents associated with the jets, which were 3D topological calorimeter clusters [17].

The analysis follows similar measurements undertaken by CDF for $p\bar{p}$ collisions [18, 19, 20], by ZEUS for $e^{\pm}p$ [21, 22, 23, 24], and OPAL for e^+e^- [25, 26] collisions.

The ATLAS analysis uses data corresponding to 3 pb^{-1} of total integrated luminosity, collected during 2010. This period of data collection can safely be referred to as ATLAS's early days, when pile-up was not the burning issue that it quickly became in 2011, after about 35 pb^{-1} had been collected. In 2010 the average number of good vertices in a single hard scatter was approximately 2. In 2011 data this average is closer to 10, and increasing with luminosity.

The measurements are carried out for jets with $p_T > 30$ GeV and $|y| < 2.8$.

The measurements of integrated and differential jet shapes, Ψ (Eq. 5) and ρ (Eq. 4), are corrected to hadron level and compared to several Monte Carlo predictions. Different phenomenological models are employed to describe the fragmentation processes and UE contributions.

The comparisons presented in [2] were complemented with additional results in a second publication [27] including the predictions from new generators and up-to-date MC tunes, and are reported in this contribution to the proceedings.

The differential jet shape $\rho(r)$ as a function of the distance $r = \sqrt{\Delta y^2 + \Delta\phi^2}$ to the jet axis is defined as the average fraction of the jet p_T that lies inside an annulus of inner radius $r - \Delta r/2$ and outer radius $r + \Delta r/2$ around the jet axis:

$$\rho(r) = \frac{1}{\Delta r}\frac{1}{N^{\text{jet}}}\sum_{\text{jets}}\frac{p_T(r - \Delta r/2, r + \Delta r/2)}{p_T(0, R)}, \ \ \Delta r/2 \leq r \leq R - \Delta r/2, \qquad (4)$$

where $p_T(r_1, r_2)$ denotes the summed p_T of the clusters in the annulus between radius r_1 and r_2, N^{jet} is the number of jets, and $R = 0.6$ and $\Delta r = 0.1$ are used.

The points from the differential jet shape at different r values are correlated since, by definition, $\sum_0^R \rho(r)\,\Delta r = 1$. Alternatively, the integrated jet shape $\Psi(r)$ is defined as the average fraction of the jet p_T that lies inside a cone of radius r concentric with the jet cone:

$$\Psi(r) = \frac{1}{N^{\text{jet}}}\sum_{\text{jets}}\frac{p_T(0, r)}{p_T(0, R)}, \ \ 0 \leq r \leq R, \qquad (5)$$

where, by definition, $\Psi(r = R) = 1$, and the points at different r values are correlated.

A summary of the results presented in [2] are given in Figure 5 for the differential jet shape in the bin 30 GeV $< p_T <$ 40 GeV and in Figure 6 for the integrated jet shape at $r = 0.3$ in jets with 30 GeV $< p_T <$ 600 GeV.

The measured jets become narrower as the jet transverse momentum and rapidity increase, although with a rather mild rapidity dependence. The results indicate that the predicted jet shapes are mainly dictated by the details of the implementation of the parton showers and the modelling of the underlying event in the Monte Carlo generators.
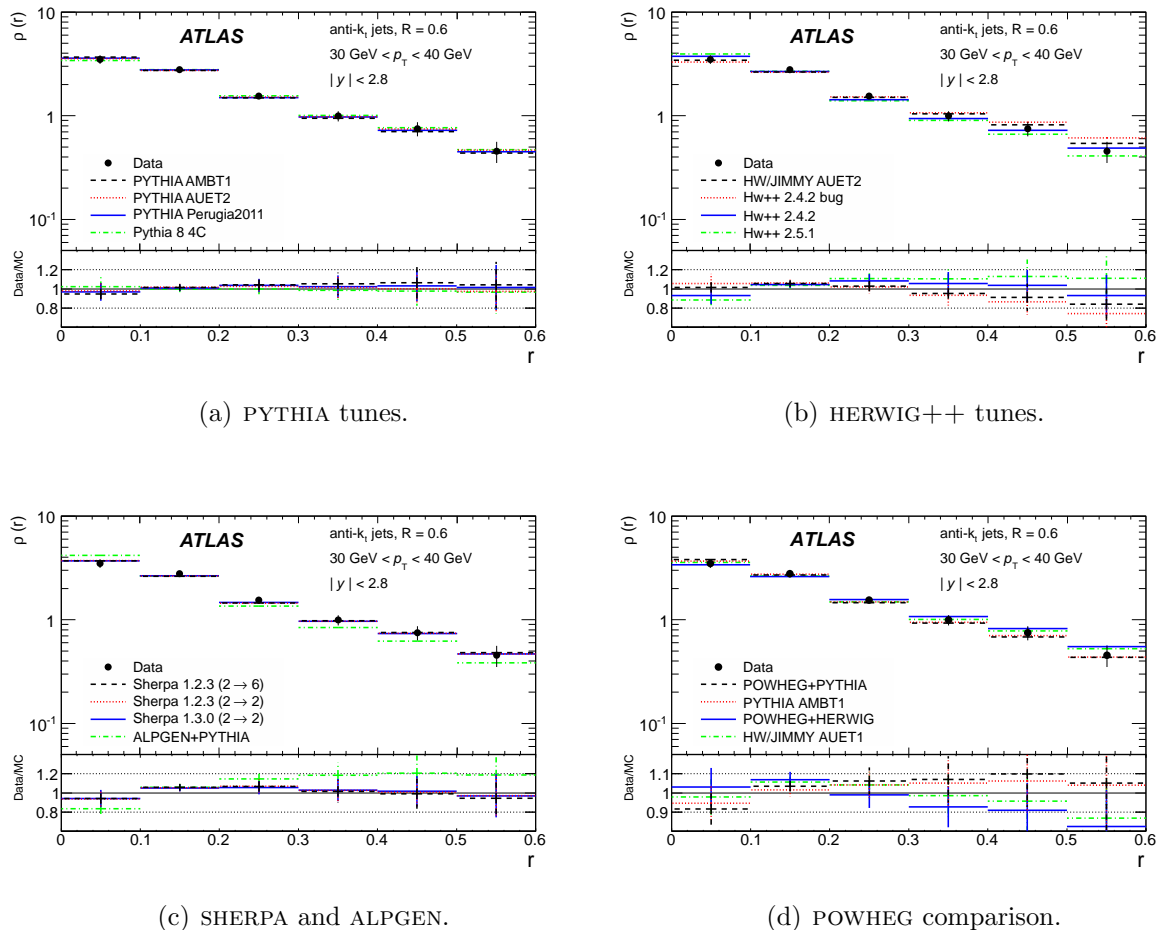
(a) PYTHIA tunes.

(b) HERWIG++ tunes.

(c) SHERPA and ALPGEN.

(d) POWHEG comparison.

Figure 5. The measured differential jet shape, $\rho(r)$, in inclusive jet production for jets with $|y| < 2.8$ and $30\,\text{GeV} < p_T < 40\,\text{GeV}$. Error bars indicate the statistical and systematic uncertainties added in quadrature. The measurements are compared to different MC predictions.

The presence of contributions from higher-order pQCD matrix elements in the final state does not affect the predicted jet shapes significantly.

The PYTHIA, HERWIG++, and HERWIG/JIMMY Monte Carlo generators, using the latest tunes to describe minimum bias and underlying-event–related observables in data, provide a good description of the measured jet shapes, although the latest version of HERWIG++ tends to produce jets narrower than the data. As expected, PYTHIA 6 AMBT1 tends to produce jets slightly narrower than the data as it underestimates the UE activity in dijet events [28] and lacks a tuned final-state parton shower from the initial-state radiation. The effect of the wrong setting in "HERWIG++ 2.4.2 bug"* is only visible for jets with $p_T < 40$ GeV.

The different SHERPA predictions are similar and provide a reasonable description

*The ATLAS Monte Carlo generation of HERWIG++ 2.4.2 had the wrong settings for parameters controlling the multiple-parton interactions.
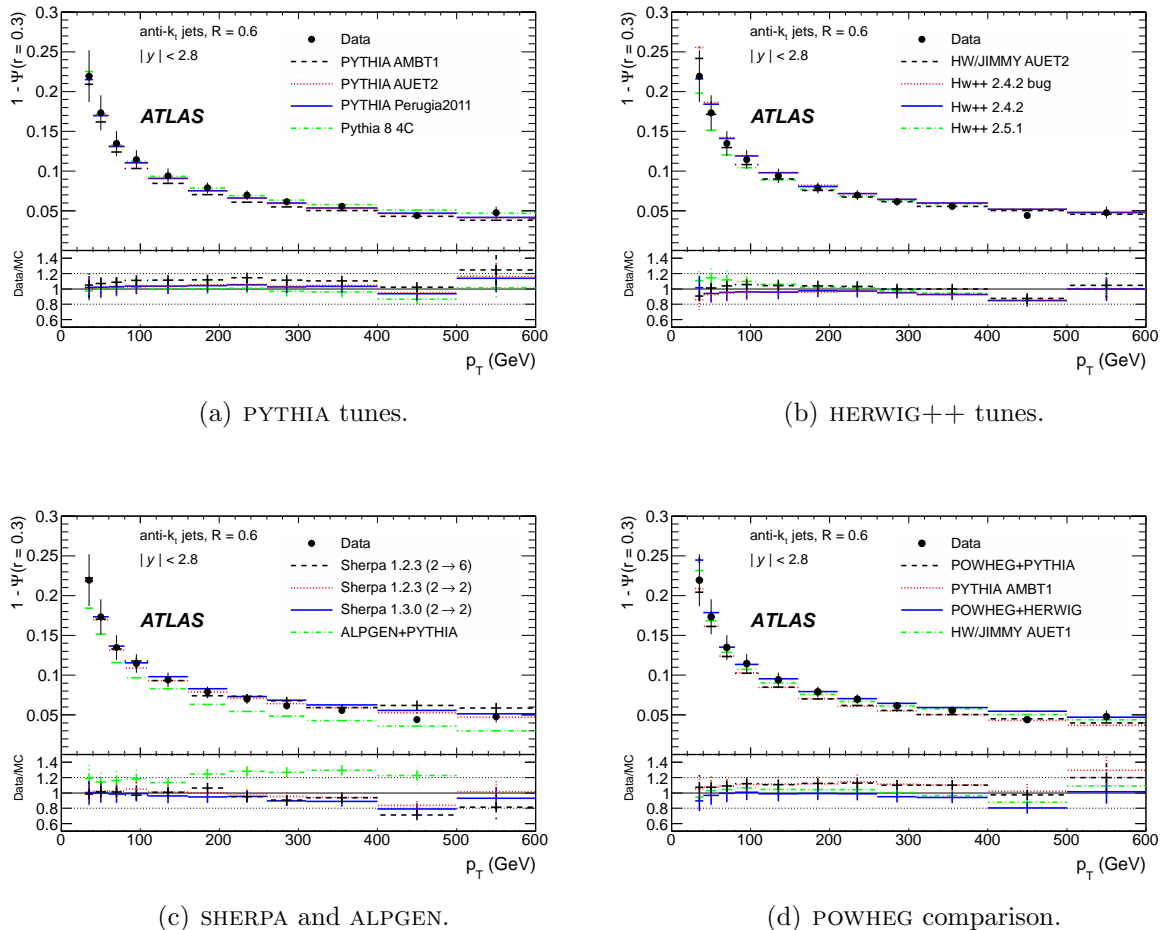
(a) PYTHIA tunes.

(b) HERWIG++ tunes.

(c) SHERPA and ALPGEN.

(d) POWHEG comparison.

Figure 6. The measured integrated jet shape, $1 - \Psi(r = 0.3)$, as a function of p_T for jets with $|y| < 2.8$ and $30\,\text{GeV} < p_T < 600\,\text{GeV}$. Error bars indicate the statistical and systematic uncertainties added in quadrature. The measurements are compared to the different MC predictions considered.

of the data. This indicates that the presence of additional partons from higher-order matrix elements contributions do not affect the predicted jet shapes, mainly dictated by the soft radiation in the parton shower. The comparison between SHERPA 1.2.3 and SHERPA 1.3.0 shows that the NLL-inspired corrections included in the latter for the parton shower do not impact significantly the predicted jet shapes. ALPGEN interfaced with PYTHIA predicts too-narrow jets and does not describe the data. This was already the case for ALPGEN interfaced with HERWIG/JIMMY [2] and requires further investigation to determine whether the disagreement observed with the data can be completely attributed to the UE modelling in the MC samples or is also related to the prescription followed by ALPGEN in merging the partons from the matrix elements with the parton showers in the final state.

Finally, POWHEG interfaced with HERWIG/JIMMY provides a reasonable description of the data while the interface with PYTHIA predicts too-narrow jets, which is mainly

attributed to the details of the underlying event modelling.

These results confirm the sensitivity jet shape measurements, and their potential to constrain different Monte Carlo models.

2.3.3. Boosted top quarks with ATLAS   First steps have been made this year by ATLAS in the quest to reconstruct the decay of a boosted top quark in a single jet. The first publication has been delivered in the context of the search for massive exotic resonances decaying to $t\bar{t}$ [29]. This analysis was able to isolate a clean sample of boosted top quarks.

Figure 7 is an event display showing a candidate boosted top quark event. The anti-k_T jets with $R = 0.4$ used in the standard ATLAS $t\bar{t}$ selection are indicated in red. The result of reclustering the constituents of these jets (topological calorimeter clusters) with $R = 1.0$ is shown in green on the same figure. For these events the three $R = 0.4$ jets that are combined to form the hadronic top candidate merge into a single jet when clustered with $R = 1.0$. These events are thus the first candidates for boosted top quarks reconstructed as single jets at ATLAS.

Although the statistics with the 2010 dataset were too low to provide a testing ground for the many substructure techniques and variables we are interested in testing on such a clean sample of boosted top quarks, the groundwork was laid down to make the prospects for boosted top analyses on 2011 data very exciting.

2.3.4. Jet substructure with ATLAS   One of the most important tasks for the early ATLAS boosted object analyses was to begin subjecting the various grooming methods and variables, initially implemented in Monte Carlo, to the tests that come with the conditions of a real detector. The recent ATLAS analysis on jet mass and substructure has done just that [4]. The analysis was based on 35 pb^{-1} of data taken in 2010 and presented the mass and splitting scale of high p_T (> 300 GeV) jets reconstructed with the anti-k_T ($R = 1.0$) algorithm and with the Cambridge-Aachen ($R = 1.2$) algorithm at different stages of grooming. The grooming method employed was a mass-drop filtering method which looks for hard subjets within the very large parent jet, and discards any radiation not falling within the subjets designated to the hard splitting. As already discussed in Section 2.3.1, the behaviour of the mass of large-area jets as a function of the number of good vertices in an event was studied and the process of filtering away the soft radiation in such jets was found to effectively remove this dependence. This is perhaps unsurprising, as the radiation present in an event due to pile-up or underlying event is expected to be a fairly soft continuum. The analysis discarded all events with more than one good vertex, focusing on the 28% of the 2010 dataset that is regarded as being free from pile-up.*

---

*The authors acknowledge that selecting on events with a single primary vertex is a limited opportunity for ignoring pile-up, as making such a demand in the 2011 data would result in approximately zero events.
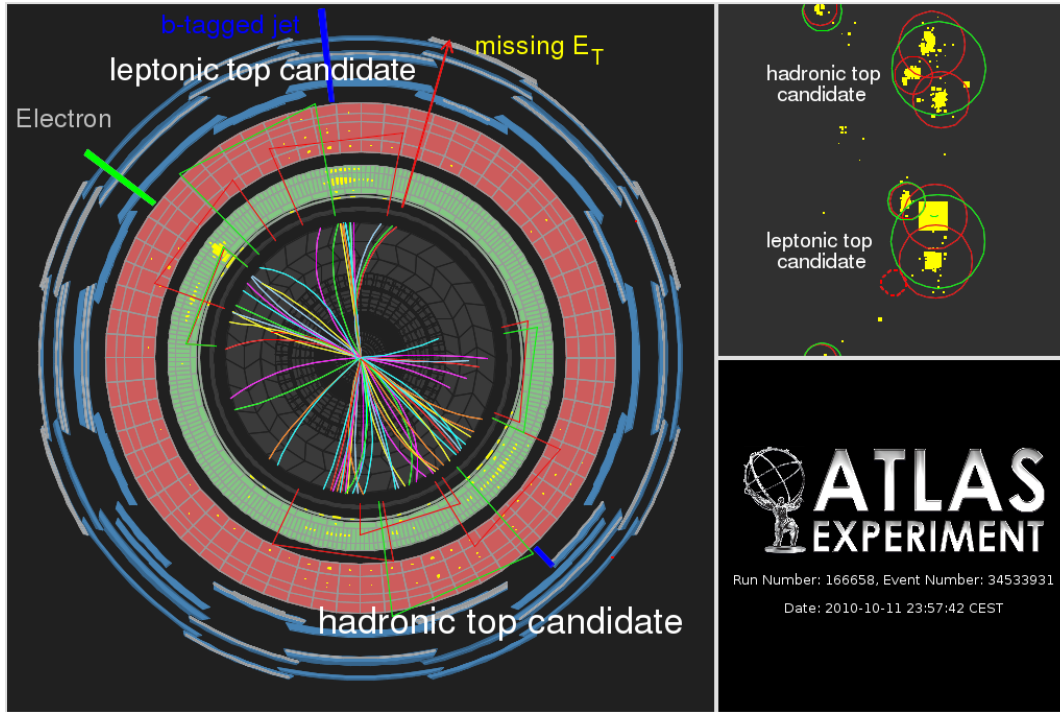
Leptonic top	E_T^{miss}: $E_T = 36$ GeV, $\phi = -1.5$
	electron: $p_T = 145$ GeV, $\eta = 1.1$, $\phi = 2.5$
	jet: $E_T = 194$ GeV, $\eta = 1.2$, $\phi = 1.7$, $m_j = 16.6$ GeV
Hadronic top	jet 2, $E_T = 155$ GeV, $\eta = 1.1$, $\phi = -0.7$, $m_j = 22.7$ GeV
($R = 0.4$ clustering)	jet 3, $E_T = 113$ GeV, $\eta = 1.3$, $\phi = -1.7$, $m_j = 14.0$ GeV
	jet 4, $E_T = 54$ GeV, $\eta = 0.6$, $\phi = -1.7$, $m_j = 8.1$ GeV
Hadronic top	jet 1, $E_T = 355.5$ GeV, $\eta = 1.3$, $\phi = -1.1$
($R = 1.0$ clustering)	$\sqrt{d_{12}} = 110$, $\sqrt{d_{23}} = 40$, $m_j = 197.1$ GeV

Figure 7. Summary table for event 34533931 of run 166658. The leptonic top candidate is formed by high-p_T electron (145 GeV, 10 o'clock), E_T^{miss} (1 o'clock), and the b-tagged jet at 12 o'clock. The three anti-k_T $R = 0.4$ jets between 4 and 6 o'clock are identified as the hadronic top candidate. When reclustered with $R = 1.0$ the three jets merge into a single jet with $m_j = 198$ GeV and subjet splitting scales $\sqrt{d_{12}} = 110$ and $\sqrt{d_{23}} = 40$ GeV.

The final distributions resulting from the analysis were unfolded to hadron level. The mass distributions of Cambridge-Aachen jets with $R = 1.2$ are shown in Figure 8 before and after employing mass-drop filtering with the requirement that the heavier subjet carry less than $\mu = 67\%$ of the mass of the parent jet and the splitting between subjets is fairly symmetric, $y_2 \equiv \frac{\min\left(p_{T,a}^2, p_{T,b}^2\right)}{m_{\mathrm{jet}}^2} \Delta R_{ab}^2 < y_2^{\mathrm{cut}} = 0.09$. Figure 9 shows the mass and splitting scale ($\sqrt{d_{12}} = \min(p_{T,a}, p_{T,b}) \times \Delta R_{ab}$) of anti-$k_T$ jets with $R = 1.0$.

In all cases the distributions are found to be well modelled by a range of leading-order parton shower Monte Carlos, to within the systematic uncertainties.
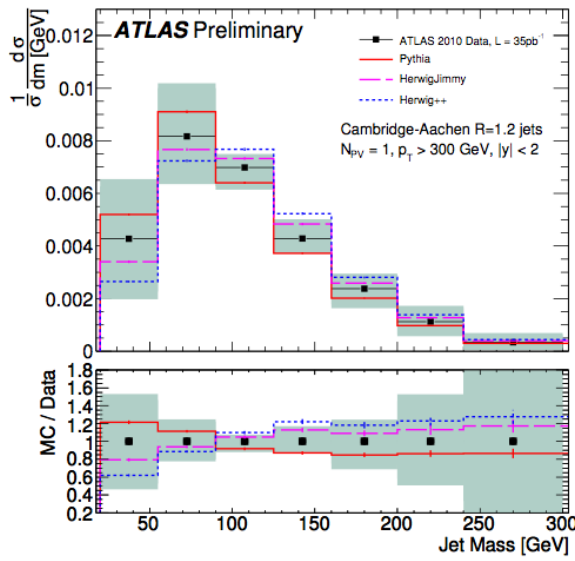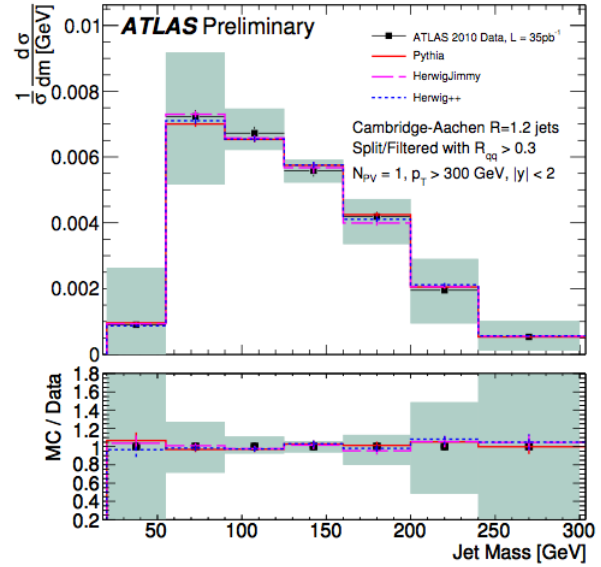
(a) C/A R=1.2 jet mass.

(b) Filtered C/A R=1.2 jet mass.

Figure 8. The invariant mass distribution of Cambridge-Aachen $R = 1.2$ jets (left) and the mass distribution after filtering (right). Both distributions are unfolded to stable-particle level and compared to PYTHIA, HERWIG, and HERWIG++. The systematic uncertainties are shown by the shaded band.

(a) Anti-k_t R=1.0 jet mass.

(b) Anti-k_t R=1.0 splitting scale.

Figure 9. The invariant mass distribution of anti-k_T $R = 1.0$ jets (left) and the splitting scale $\sqrt{d_{12}}$ of the same jets (right). Both distributions are unfolded to stable-particle level and compared to PYTHIA, HERWIG, and HERWIG++. The systematic uncertainties are shown by the shaded band.
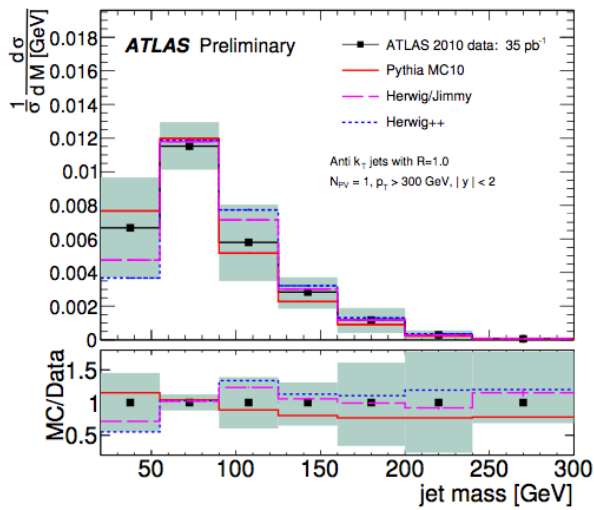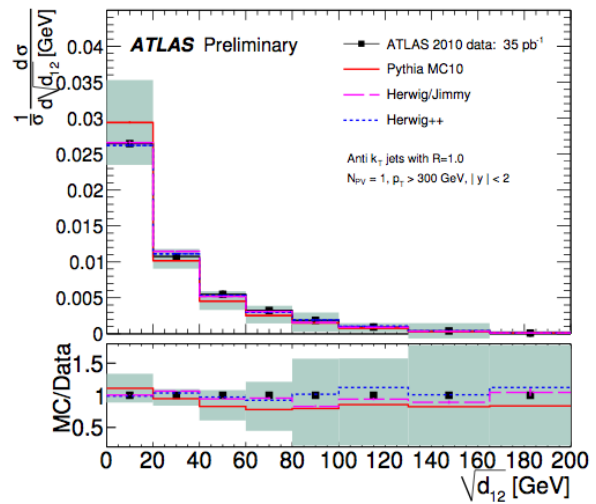
2.4. Results from CMS

2.4.1. CMS and pile-up One advantage of the CMS detector and reconstruction pipeline is the so-called "particle flow" algorithm for a more holistic approach to jet reconstruction. Because of this approach, it is possible to remove around 60% of the pile-up from jets directly as it corresponds to charged tracks which can be associated to subleading primary vertices. This aids in the reduction of pile-up in jets with substructure at CMS, and studies show that there is only moderate dependence of the substructure variables on pile-up for the luminosities considered [5].

The CMS collaboration plans to retain a data-driven approach to measuring mis-tag rates, ameliorating pile-up issues there. Further studies are ongoing to utilise other advanced jet reconstruction techniques to further reduce pile-up dependence.

2.4.2. Jet Shapes with CMS Several jet shape measurements have been performed at CMS similar to those at ATLAS described above in Section 2.3.2. The first is the examination of the classic jet shapes, and the second is the examination of the jet charged component structure, both in [3].

Several differences exist between the ATLAS and CMS results. While both collaborations use the anti-k_T jet algorithm, CMS uses different values of the radius parameter, R. For the inclusive shape measurements, two types of jets were used: calorimeter-only jets and jets where the calorimeter response was corrected using associated tracks ("jet-plus-tracks" jets) [30]. To reduce out-of-cone radiation, a large R of 0.7 was used. The jets were required to have (track-corrected) transverse momenta greater than 15 GeV. For the charged multiplicity measurement, only the jet-plus-tracks jets were used, with $R = 0.5$. The (track-corrected) transverse momenta for the first two jets were required to be larger than 20 and 10 GeV, respectively.

The distribution of $\Psi(r)$ (Eq. 5) is shown in Figure 10. The Monte Carlo simulation is doing a very reasonable job at predicting the data, and the agreement improves with larger transverse momentum.

2.4.3. Boosted top quarks and W bosons with CMS CMS has developed algorithms to identify the hadronic decays of boosted top quarks and W bosons. The top-tagging algorithm is based on the Johns Hopkins tagger [31], with small modifications as described in [32, 1]. The W-tagging algorithm is based on jet pruning [33, 34], adding a requirement on the mass drop of the subjet splitting, which was motivated by the BDRS subjet/filter algorithm [35].

The algorithms were characterised as of the BOOST 2011 conference [5], and subsequent studies have advanced this characterisation [36]. The strategy for the studies here is to have data-driven mis-tag predictions which can accurately represent non-top and non-W backgrounds. Sidebands in the data are selected that have little to no true top or W contributions, and the tagging rate is derived as a function of the jet transverse momentum. These per-jet parameterisations are then applied to each jet in
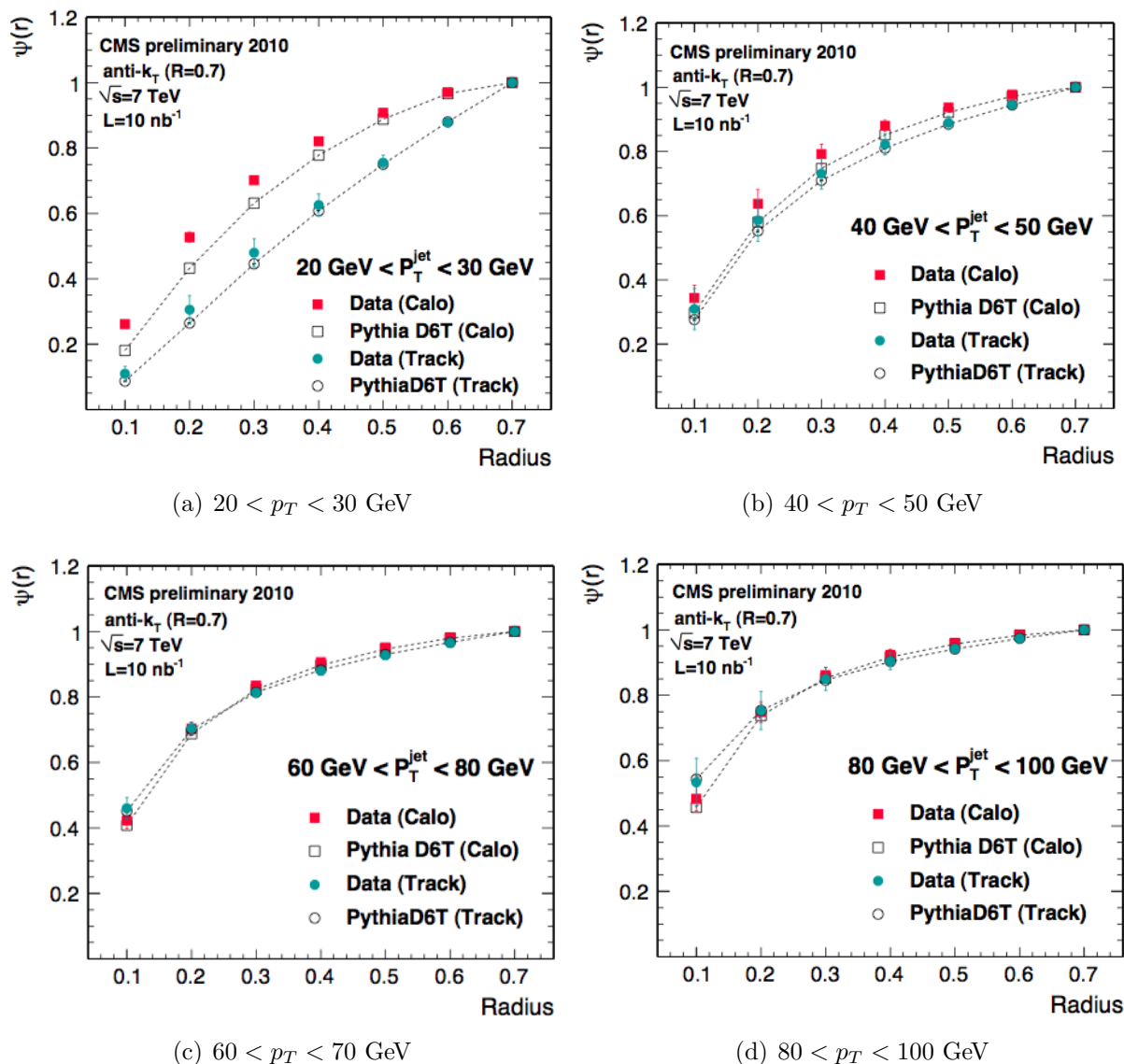
(a) $20 < p_T < 30$ GeV

(b) $40 < p_T < 50$ GeV

(c) $60 < p_T < 70$ GeV

(d) $80 < p_T < 100$ GeV

Figure 10. The measured differential jet shape at CMS, $\rho(r)$, in inclusive jet production for jets with $p_T > 15$ GeV. Error bars indicate the statistical and systematic uncertainties added in quadrature. The measurements are compared to MC predictions in different p_T bins.

a signal selection, which is used to form a data-driven background estimate. This has several advantages, primarily that modelling effects are not relevant. Moreover, pile-up effects are handled directly, because the same data sample is used in the sidebands and the signal region, so the pile-up contribution is the same.

The efficiency for the tagging algorithms is derived from Monte Carlo, and corrected for a data-to-Monte-Carlo scale factor using Standard Model $t\bar{t}$ events in the semi-leptonic channel in [36]. In that public result, limits are set on the possible cross section for narrow resonances decaying to $t\bar{t}$ pairs.

Figure 11 shows the mis-tag rates and efficiencies for the top and W tagging
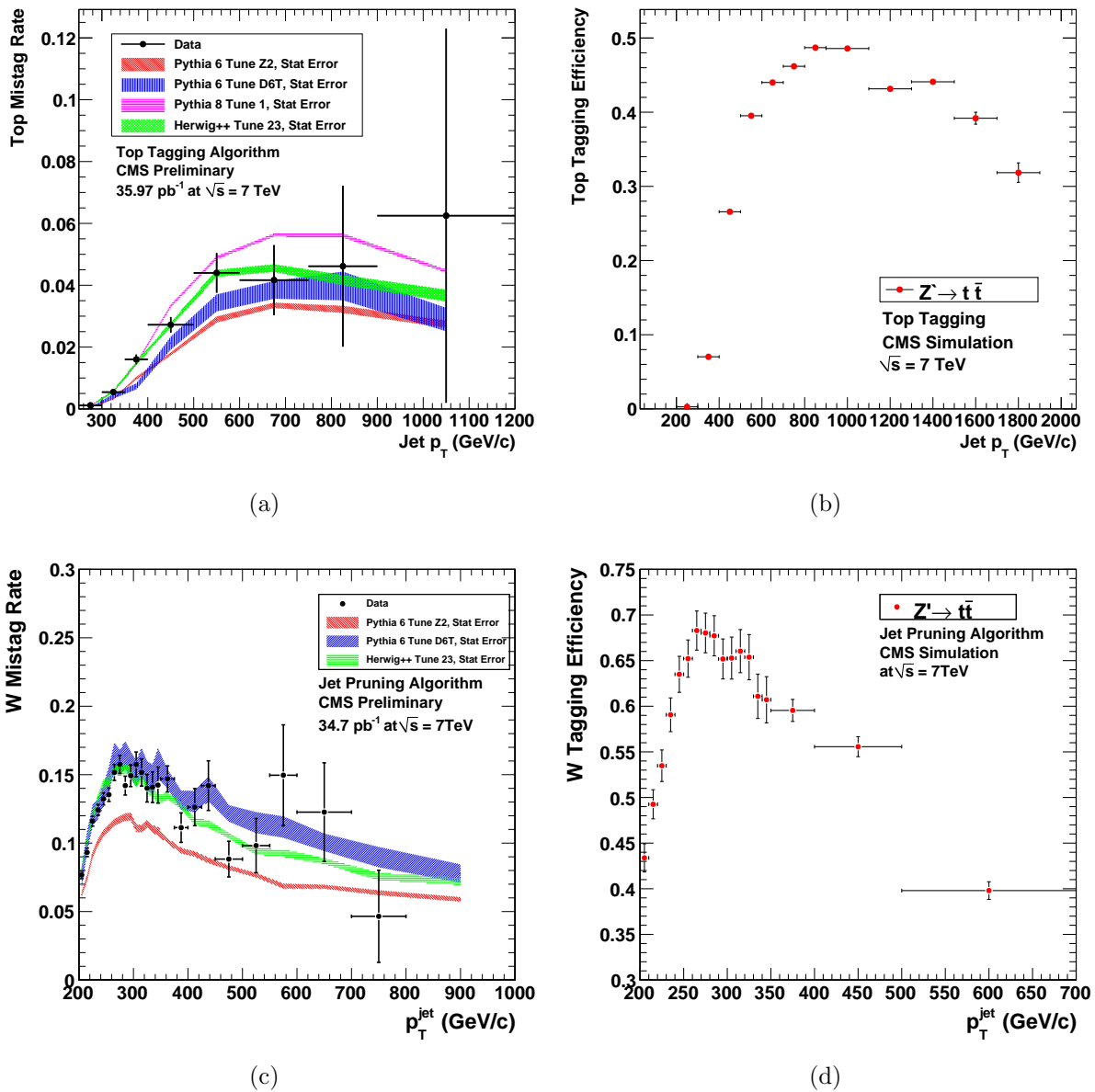
algorithms from CMS.

(a)   (b)

(c)   (d)

Figure 11. Mis-tag rates and efficiencies for the top tagging (top) and *W* tagging (bottom) algorithms. The mis-tag rates are measured in a signal-depleted control sample and compared to PYTHIA and HERWIG++ predictions. The efficiencies for tagging top quarks and Ws are estimated from PYTHIA simulation.

2.4.4. Jet substructure at CMS The study of the performance of jet substructure techniques in generic QCD samples is critically important to understand these algorithms, and to derive appropriate sideband regions for data-driven background estimates at CMS. As such, CMS has performed detailed comparisons of jet substructure observables in [5].

For example, Figure 12 shows the jet mass for the top-tagging and W-tagging algorithms, compared to several different predictions from Monte Carlo. The simulation seems to be predicting the data quite nicely for all of the generators examined, with slight variations based on shower model and underlying event tunes. This seems to have a much larger effect on the substructure than the pile-up contributions.
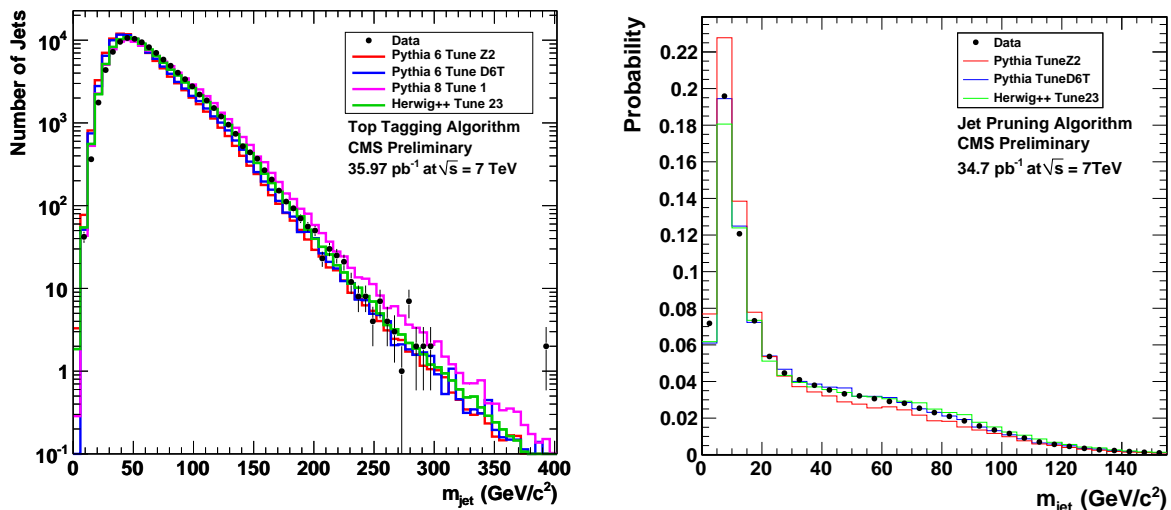
(a) Top-tagged jet mass.

(b) W-tagged jet mass.

Figure 12. The jet mass distribution obtained with the top-tagging algorithm (left) and the W-tagging algorithm using jet pruning (right). Data are compared to PYTHIA and HERWIG++.

3. New tools and techniques

Jet substructure techniques attempt to extract additional information about a jet from a detailed study of its constituents. These methods have been mainly aimed at distinguishing boosted hadronic objects like top quarks and W/Z/Higgs bosons from the background of jets initiated by light quarks and gluons. Many such techniques exist, and to help make sense of them, the BOOST 2010 report [1] proposed that they be classified according to three broad categories: (1) methods that directly identify subjets within a jet, (2) methods which "groom" away uncorrelated radiation within a jet, and (3) methods based on energy flow within a jet.

Since the BOOST 2010 workshop, a variety of new techniques have been introduced which will be described in more detail below. A recent and thorough review of substructure techniques applied to top tagging can be found in [37]; here we focus on the developments since BOOST 2010. N-subjettiness [38, 39] and dipolarity [40] are examples of hybrid jet shapes, which describe the energy flow of a jet (as in method (3) above) with respect to candidate subjet axes (determined using e.g. method (1) above). Jet substructure through angular correlation functions [41] is a complementary

technique to energy flow observables. The template overlap method [42] and the shower deconstruction method [43] classify jets with the help of approximations to hard matrix elements and the parton shower. Beyond the highly boosted regime, the HEP (Heidelberg-Eugene-Paris) top tagger [44] is appropriate for identifying moderately boosted top quarks. Meanwhile, substructure techniques have been been used in a variety of interesting applications, including separating quark jets from gluon jets [45, 46], tagging jets from initial state radiation [47], and identifying boosted decay products of new physics [48, 49].

3.1. N-subjettiness

In [38], Thaler and van Tilburg introduced a new jet shape "N-subjettiness" (denoted τ_N), designed to identify boosted N-prong hadronic decays. N-subjettiness quantifies the degree to which jet radiation is aligned along specified subjet axes, such that small values of τ_N correspond to N or fewer subjets, while large values of τ_N indicate more than N subjets. This jet shape was adapted from the event shape N-jettiness introduced in [50] to define exclusive jet cross sections, and similar ideas were pursued by Kim in [39].*

Given candidate subjet directions determined by an external algorithm (such as the exclusive k_T procedure [51, 52]), τ_N is defined as

$$\tau_N = \frac{\sum_k p_{T,k} \left(\min \left\{ \Delta R_{1,k}, \Delta R_{2,k}, \ldots, \Delta R_{N,k} \right\} \right)^\beta}{\sum_k p_{T,k} (R_0)^\beta}, \tag{6}$$

where the sum runs over the particles in the jet, $p_{T,k}$ is the transverse momentum of particle k, $\Delta R_{A,k}$ is the azimuth-rapidity distance between subjet axis A and particle k, and R_0 is the characteristic jet radius defined such that $0 \leq \tau_N \leq 1$. The constant β is an angular weighting exponent closely related to angularities [53], and 1-subjettiness roughly corresponds to jet angularities [54] with $a \equiv 2 - \beta$.

To separate boosted hadronic objects from the QCD jet background, one could use the complete set of τ_N values (with different values of β) in a multivariate analysis. However, [38] showed that a simple cut on the ratio τ_N/τ_{N-1} provides excellent discrimination power for N-prong hadronic objects. In particular, τ_3/τ_2 is a successful boosted top discriminator, and τ_2/τ_1 can identify boosted W/Z and Higgs bosons, with the angular weighting exponent $\beta = 1$ (corresponding roughly to jet broadening [55]) providing the best discrimination. In subsequent work [56], Thaler and van Tilburg showed that the initial step of choosing candidate subjet axes is in fact unnecessary. In particular, the quantity in Eq. 6 can be minimised over the candidate subjet directions using a variant of the k-means clustering algorithm [57], further improving boosted object discrimination.

---

*[39] focused on boosted Higgs identification, using a Lorentz-invariant version of N-subjettiness defined in the jet rest frame.

3.2. Dipolarity

A new colour flow observable, "dipolarity", was introduced by Hook, Jankowiak, and Wacker to discriminate between different colour configurations of a given pair of subjets j_1 and j_2 [40]. Dipolarity is given by a sum in which each constituent of j_1+j_2 is weighted by its p_T and its squared angular separation ΔR^2 from the line segment connecting j_1 and j_2 in the η-ϕ plane:

$$\mathcal{D} \equiv \frac{1}{\Delta R_{12}^2} \sum_{i \in J} \frac{p_{Ti}}{p_{T_J}} \Delta R_i^2. \tag{7}$$

For subjets j_1 and j_2 in a colour singlet configuration, the radiation pattern is of the dipole form with most radiation clustered in the region between the two subjets. Consequently $\mathcal{D}$ is expected to be small for colour singlet configurations and larger for other colour configurations, in which j_1 and j_2 are colour connected to other subjets.

By considering the entire radiation pattern of the two subjets at once, dipolarity is designed to be most effective in the semi-boosted regime, where there can be considerable overlap between the two subjets. This is in contrast to jet pull [58], which was introduced with the low boost regime in mind and which can lose discrimination power if there is substantial overlap. As a first application, dipolarity has been incorporated into the HEP top tagger [44], where it was shown to improve background rejection by probing the colour structure of the reconstructed W boson. More work will be needed to determine whether dipolarity can be applied effectively outside of top tagging.

3.3. Jet substructure without trees

Jankowiak and Larkoski developed a method for identifying substructure within jets via angular correlations [41], introducing an angular correlation function $\mathcal{G}(R)$:

$$\mathcal{G}(R) \equiv \frac{\sum\limits_{i \neq j} p_{Ti} p_{Tj} \Delta R_{ij}^2 \Theta(R - \Delta R_{ij})}{\sum\limits_{i \neq j} p_{Ti} p_{Tj} \Delta R_{ij}^2}, \tag{8}$$

where the sum runs over all pairs of jet constituents. The angular correlation function (ACF) measures the contribution to a jet's mass from pairs of constituents separated by an angular scale R or less. A high-p_T QCD jet has an ACF that goes approximately like a power of R, since it is nearly scale-invariant. By contrast, a jet initiated by a heavy particle decay has one or more intrinsic scales, which results in an ACF with one or more "cliffs".*

For a given jet, numerous infrared/collinear-safe observables can be constructed from the ACF, and these can be used to characterise the jet's substructure. For example, one can look at the angular scales at which cliffs are located as well as the corresponding

---

*For example, consider a jet with two well-defined narrow subjets. Its ACF will increase steeply near R_{sub}, where R_{sub} is the subjet separation, since pairings of constituents from each subjet begin to contribute to the sum in Eq. 8 for $R \gtrsim R_{sub}$.

cliff heights. Cliff heights are closely related to mass drops as utilised in BDRS mass-drop/filtering [35] and can be used to extract mass scales that correspond to hard substructure in the jet. As a first application of these ideas, Jankowiak and Larkoski developed a top tagging algorithm whose performance is competitive with others in the literature. Other applications remain to be explored. Further work on these ideas was pursued in [59].

3.4. Template overlap

The energy distribution resulting from hard scatterings can be well described by energy correlation functions in momentum space. In QCD, these naturally describe jet cross sections in terms of energy flow observables, which are peaked around the states associated with the hard scattering that subsequently initiate the jets. Therefore, energy flow observables within the jet should be of particular interest to substructure studies. In [42], Almeida, Lee, Perez, Sterman, and Sung developed a method based on the quantitative comparison of the energy flow of observed jets at high-p_T with the flow from selected sets (the templates) of partonic states.

The template overlap procedure can be summarised as follows. Let $|j\rangle$ denote the set of particles or calorimeter towers that make up a jet, identified by some algorithm, and take $|f\rangle$ to represent a set of partonic momenta $p_1 \ldots p_n$ that represent a boosted decay, found by the same algorithm. The functional measure $\mathcal{F}(j, f) \equiv \langle f|j\rangle$ quantifies how well the energy flow $|j\rangle$ matches the (templates) $|f\rangle$. In practice, [42] found good results with a simple construction of functional overlap based on a Gaussian in energy differences within angular regions surrounding the template partons. Any region of partonic phase space for the boosted decays, $\{f\}$, defines a template. Knowledge of the signal and background can be used to design a custom analysis for each resonance, to make use of differences in energy flow between signal and background. The template overlap of an observed jet j is the defined as $Ov(j, f[j]) = \max_{\{f\}} \mathcal{F}(j, f)$, the maximum functional overlap of j to a state $f[j]$ within the template region, where $f[j]$ stands for the state of maximum overlap, emphasising that the value of the overlap functional depends not only on the physical state $|j\rangle$, but also on the choice for the set of template functions f.

Template overlaps provide a tool to match unequivocally arbitrary final states j to partonic partners $f[j]$ at any given order. Once a "peak template" $f[j]$ is found, it can be used to characterise the energy flow of the state, which gives additional information on the likelihood that it is signal or background. In addition, template overlaps can be combined with higher moments of the energy distribution or jet shapes to further discriminate the event.

3.5. Shower deconstruction

Shower deconstruction, proposed by Soper and Spannowsky, is a method to look for new physics in a hadronic environment [43]. First, one picks the part of the event

that is likely to be of interest, for instance the part contained in a large-radius jet that possibly contains the decay products of a boosted heavy particle. This part of the event is divided into small radius jets called the microjets that are ideally the size of topoclusters or calorimeter towers. If there are too many microjets to analyse, one can discard the microjets with the lowest transverse momenta. Shower deconstruction uses the four-momentum and possibly b-tag information for each microjet.

The aim of shower deconstruction is to calculate a single number χ for each event such that events with small χ are likely to be background events and events with large χ are likely to be signal events. The number χ is an approximation to the ratio $P(S)/P(B)$ of the probability $P(S)$ that a parton shower Monte Carlo that represents the sought signal process would generate the given event to the probability $P(B)$ that a parton shower Monte Carlo that represents the background process would generate the event. The function $P(S)$ is calculated as of a sum, over all possible shower histories for the signal hypothesis, of weights that are a product of splitting-kernels and Sudakov factors. $P(B)$ is calculated the same way, but for the background hypothesis.

Although shower deconstruction is not limited to boosted configurations, the computing time increases strongly with the number of microjets. Boosted configurations are known to ameliorate combinatoric problems in reconstructing a resonance that decays hadronically because all decay products can be in one wide angle jet. Thus, [43] presents a first application of shower deconstruction using the HZ production channel, where the boosted Higgs decays to a $b\bar{b}$ pair, first discussed in [35]. The statistical significance obtained with the shower deconstruction algorithm is found to be larger than that obtained with the method of [35].

3.6. HEP top tagger

Unlike other taggers, the HEP top tagger, proposed by Plehn, Salam, and Spannowsky, is not motivated by searches for resonances decaying to two highly relativistic top quarks [44]. Instead, its first application was the notorious Higgs search channel $pp \rightarrow t\bar{t}H$ with a hadronically decaying $H \rightarrow b\bar{b}$ [35]. In the Standard Model, one can expect several percent of the events to have transverse momenta in the range $p_{T,H} \gtrsim m_H$ and $p_{T,t} \gtrsim m_t$, for the leading hadronically decaying top quark. To extract the $t\bar{t}H$ signal from the continuum QCD background, [44] required two fat jets, one from a boosted Higgs and one from a boosted top quark.

Another application of top tagging in a moderately boosted regime is identifying top partners—like a supersymmetric top squark—decaying to a top quark and an invisible dark matter agent [60]. Similar to the $t\bar{t}H$ channel such searches suffer from combinatoric backgrounds. Using this tagger, one can exploit purely hadronic top decays and extract the stop pair signal out of backgrounds.

Algorithmically, the HEP top tagger is motivated by the BDRS Higgs tagger. In particular, it starts with a large, $R = 1.5$, Cambridge-Aachen jet. This size immediately translates into a minimum transverse momentum condition of $p_{T,t} \gtrsim 200$ GeV. This fat

jet is unclustered using an iterative mass-drop criterion, with a general cutoff at $m_{\bar{j}} > 30$ GeV for the subjets. Next, filtering [35] is applied to sets of three hard subjets, using five constituents, and a combination of three subjets is chosen with jet mass closest to the top mass. To reconstruct the W mass, notice that for the top decay kinematics, it is surprisingly likely that more than one of the three m_{jj} combinations lies within 15% of the W mass. Therefore, the HEP top tagger does not aim to distinguish the b jet from the two W decay jets, but instead applies a more democratic subjet mass criterion described in [60]. Finally, a self-consistency condition is applied on the reconstructed transverse momentum $p_{T,t} > 200$ GeV.

In a recent application, Plehn, Spannowsky, and Takeuchi studied semi-leptonic decays of top partners into two top quarks and missing energy [61]. The hadronic top was reconstructed with the usual tagging algorithm. For the leptonic top, the unmeasured neutrino three-momentum was reconstructed based on the assumption of a boosted top decay. Two of the three unknown components can be reconstructed using the top and W mass constraints. For the third component, one can analyse the top decay in a specific rest frame and find that one of the neutrino momentum components is strongly suppressed. This way, one can approximately reconstruct the neutrino momentum and compare it to the measured two-dimensional missing transverse momentum vector. The results for supersymmetric top squarks are promising over a wide range of masses with a similar reach in the hadronic and semi-leptonic channels.

As this report was in preparation, several further extensions of the HEP top tagger were proposed [62].

3.7. Quark vs. gluon separation

Being able to distinguish light-quark jets from gluon jets on an event-by-event basis could significantly enhance the reach of many new physics searches at the LHC. The two prongs of this effort are finding intra-jet observables whose distributions are significantly different between the flavours, and finding relatively pure samples of quark and gluon jets to measure these observables in data. Identifying quark and gluon jets was also studied by ATLAS in the context of reducing jet energy scale uncertainty [63].

In [45], Gallicchio and Schwartz systematically examined many existing and novel jet substructure observables to find the ones whose distributions, for a given jet η and p_T, are the most powerful single and multi-variable discriminants. It turned out that a combination of the charged track multiplicity and the p_T-weighted linear radial moment (girth) performed almost as well on particle-level Monte Carlo as discriminants with more variables. Over 95% of the gluon jets can be filtered out while keeping more than half of the light-quark jets.

The best single observable was the number of charged particles within the jet (which were required to have $p_T > 500$ MeV). The discrimination power improved with jet p_T, and the strength relative to other observables was greatest at high signal efficiency, where mild cuts were required.

Another good single variable, and part of the best pair, was the linear radial moment — a measure of the "width" or "girth" of the jet — constructed by adding up the p_T deposits within the jet, weighted by distance from jet axis. It is defined as

$$g = \sum_{i \in \text{jet}} \frac{p_T^i}{p_T^{\text{jet}}} |\Delta R_i| \tag{9}$$

where $\Delta R_i = \sqrt{\Delta y_i^2 + \Delta \phi_i^2}$ and where the true boost-invariant rapidity y should be used when measuring with respect to the (massive) jet axis instead of the geometric pseudorapidity η. This is a boost-invariant version of jet broadening, to which it reduces in the limit of massless constituents at small angles to the jet axis.

Finding relatively pure samples was discussed by Gallicchio and Schwartz in [46]. Such samples are necessary because all intra-jet observables have distributions with significant overlap between quark and gluon jets. Combined distributions of an evenly mixed sample do not provide verification, independently for quarks and gluons, of the showering and detector simulation.

Kinematic cuts on multijet and jets+X tree-level samples were optimised to purify first quarks, then gluons. At the 7 TeV LHC, the $pp \to \gamma + 2$ jets sample can provide 98% pure quark jets with 200 GeV of transverse momentum and a cross section of 5 pb. To get 10 pb of 200 GeV jets with 90% gluon purity, the $pp \to 3$ jets sample can be used. These samples could provide a direct evaluation of the tagging technique at all jet p_T's, verify and help improve the Monte Carlo generators, and provide a test of perturbative QCD.

3.8. ISR tagging

In [47], Krohn, Randall, and Wang studied the feasibility of identifying jets from initial state radiation (ISR) on an event-by-event basis, and considered how these jets can be used in the interpretation of new physics phenomena. As a proof of principle, they investigated the pair production of new physics states which each decay into jets and missing energy, and suggested that ISR can be identified by looking for jets which are distinguished in either their p_T, rapidity, or m/p_T ratio. Using these three criteria they report that they can identify ISR in di-squark (di-gluino) events roughly 40% (15%) of the time with a mis-tag rate of around 10% (15%).

The most obvious application of the technique is in reducing the combinatoric difficulties which arise in event reconstruction. However, the production of ISR is governed by the detailed properties of a hard scattering event, e.g., the flavour of the initial partons and the scale of the hard interaction, and so ISR can be used to distinguish between different production mechanisms yielding events with similar visible final states. In [47], the authors provide an example of this, showing how one can, over many samples, observe the recoil of a new-physics system against ISR and thus infer the mass scale of the system even in the presence of significant missing energy.

3.9. Multitagging for New Physics

The application of one or more boosted object taggers can also be used effectively in searches for the tagged objects *within* new physics event samples themselves. This provides the potential to discover the Higgs boson in a way distinct from Standard Model search strategies, as well as characterising the interactions of the new physics by understanding the variety of boosted objects that appear in these samples. Kribs, Martin, Roy, and Spannowsky demonstrated that a slightly modified BDRS algorithm [35] was highly effective at finding the lightest supersymmetric Higgs boson in superpartner-enriched event samples, where a boosted Higgs boson appeared in the cascade from heavy supersymmetric particles decaying to light supersymmetric particles with a gravitino [48] or neutralino [49] lightest supersymmetric particle. Vector-like fermionic top partners also provide a rich final state amenable to the simultaneous application of multiple boosted object taggers. Top-partners decay $t' \to (bW, tZ, th)$ with roughly $(50\%, 25\%, 25\%)$ branching ratios [64]. Kribs, Martin, and Roy showed that combining both the HEP top tagger [44] with the BDRS algorithm [35] could identify both boosted t, boosted h, as well as boosted W/Z (though modified filtering/subjet techniques). This was shown to be highly effective at identifying top partners with the Higgs boson in LHC simulations.

4. Jet substructure in FastJet 3

One of the aims of FastJet 3, available since October 2011 from http://fastjet.fr/, is to facilitate the use and development of jet substructure tools. A novelty relative to the 2.X series is that jets are now "self-aware". So whereas previously one would access a jet's constituents via its cluster sequence

```
vector<PseudoJet> constituents = cluster_sequence.constituents(jet);
```

one may now write

```
vector<PseudoJet> constituents = jet.constituents();
```

and similarly for other properties such as parents, subjets and, where relevant, areas. Aside from being more intuitive to write, this also has the advantage that when dealing with multiple cluster sequences, one no longer needs to remember which cluster sequence to use with which jet.

In FastJet 2.X, the only way in which one could create an object with substructure was by creating a cluster sequence for it. Accordingly a number of tools were written as plugins, which wasn't necessarily the most natural way of formulating them. In FastJet 3, an easy way of creating substructure is via the "join" function. Suppose one has `W1`, `W2` and `b` subjets obtained from some declustering procedure. Then one may simply write

```
PseudoJet W = join(W1,W2);
PseudoJet top = join(W, b);
```
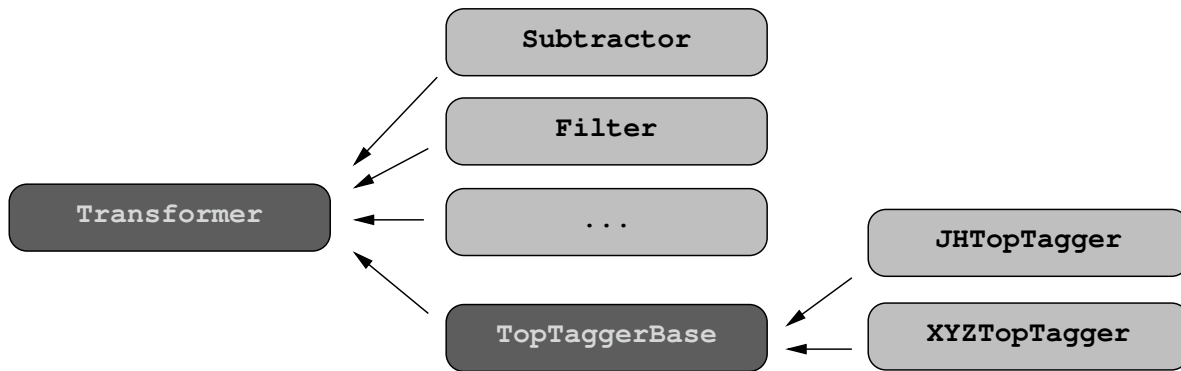
Figure 13. Illustration of some of the classes deriving from `Transformer` in FastJet 3. Classes shown in dark grey are abstract base classes.

Then, not only will the top's momentum be sensible, but `top.constituents()` will return the concatenation of the constituents of `W1`, `W2` and `b`. The high-level top substructure can be accessed with

```
vector<PseudoJet> top_pieces = top.pieces()
```

where the vector contains the `W` and the `b`. The `pieces()` function also works on normal jets from a cluster sequence.

A number of substructure tools are distributed with FastJet 3. They derive from the `Transformer` class, and top taggers should derive from `TopTaggerBase`, as shown in Figure 13. As an example consider the `Filter` class, which can be used as follows:

```
#include "fastjet/tools/Filter.hh"
#include "fastjet/Selector.hh"
double Rfilt = 0.3;
Selector selector_filter = SelectorNHardest(3);
Filter filter(Rfilt, selector_filter);
PseudoJet filtered_jet = filter(jet);
```

Note the use of the `Selector` (itself new to FastJet 3), which provides an easy way of specifying the cuts on the subjets and passing them to the `Filter` class. Simply changing the selector leads to trimming [65]

```
Selector selector_trimmer = SelectorPtFractionMin(0.05);
Filter trimmer(Rfilt, selector_trimmer);
PseudoJet trimmed_jet = trimmer(jet);
```

Transformed jets often have more internal structure than a normal jet. In the case of trimmers and filters, for example, one may want to know which subjets did not pass the selection. For this purpose there is the `structure_of<TransformerName>()` function, which returns a reference to a transformer-specific class with extra information about the jet, e.g.,

```
vector<PseudoJet> rejected_subjets =
                  filtered_jet.structure_of<Filter>().rejected();
```

Other substructure tools that are part of FastJet 3 include a `Pruner` [34], a `MassDropTagger` [35], a `JHTopTagger` [31], and a `RestFrameNSubjettinessTagger` [39]. Given the rapid evolution of the substructure field, it is not realistic for FastJet to always distribute a complete and up-to-date set of substructure tools. Accordingly, in the near future we envisage setting up a FastJet "contrib" area to facilitate dissemination of third-party tools.

FastJet 3 also contains changes unrelated to substructure. These include a new interface to pile-up and underlying background estimation, including a new and very fast grid-based median background estimator. Also of use is a new facility for attaching arbitrary user information to jets, beyond just the `user_index` of FastJet 2.X. Illustrations of its usage together with HepMC and Pythia 8 are available on request from the FastJet authors. More information on these and other developments is to be found in the FastJet manual, as well as the slides and doxygen documentation on the FastJet web site [66].

5. Benchmark samples and comparisons

As proposals proliferate for LHC searches with jet substructure, the space of questions to ask about substructure techniques grows correspondingly larger. Which techniques work best for which signals? Does the answer depend on the p_T of particles in question, or whether the analysis is a search or a measurement? How do detector limitations and uncertainties affect each method? How do things change as the amount of pile-up present increases? If we study these questions with Monte Carlo event generators, do the answers depend on which generator we choose?

In this section we will address a few of these questions. Beyond the specific results we give, we hope that the set of samples and tools we use will provide a starting point for future work. The results here can then be seen as benchmarks for comparison.

Our starting point is the set of comparisons presented in the BOOST 2010 report [1]. That analysis compared top taggers exclusively for several reasons. A large number of substructure techniques are either designed for finding tops or can be used that way; the two-step decay of a top quark is an interesting example to study; and finding top jets is immediately useful at the LHC. For the same reasons, as well as limited time and space, we will take the same approach and focus on distinguishing top jets from pure QCD background.∗ Extending last year's results, we will consider new techniques, more Monte Carlo generators — including matched samples, and the effects of a simple detector model.

Samples new and old are publicly available at

http://tev4.phys.washington.edu/TeraScale and

http://www.hep.louisville.edu/~verm/TeraScale.

∗A thorough exploration of substructure methods for identifying W jets can be found in [67].

5.1. New samples

This year we expand the set of benchmark samples with events generated by the SHERPA and HERWIG++ Monte Carlos. The SHERPA events allow us to examine the effects of higher-order matrix elements, which should provide a more accurate description of hard QCD radiation. The HERWIG++ events are a useful cross-check of last year's parton-shower–level results using a current-generation program.∗

5.1.1. Matched samples with SHERPA We consider LHC proton-proton collisions at a center-of-mass energy of 7 TeV. We have simulated the Standard Model processes $t\bar{t} + X$, $W/Z + X$ and pure QCD jets. All samples were produced with version 1.3.1 of the SHERPA event generator [68, 69]. For the electroweak gauge bosons as well as the top-quarks we consider fully hadronic decays only. For each process we generated samples of 100,000 unweighted events for p_T slices of 100 GeV between $0 \ldots 1.6$ TeV, resulting in an almost flat p_T distribution when combining all samples. As slicing parameter we used the maximum of the Monte Carlo top/anti-top p_T, the gauge-boson p_T for the W/Z channels, and the leading-jet p_T for pure jet production, where parton-level jets were reconstructed according to the anti-k_T algorithm with $R = 1.5$. For all processes the slicing cut is applied at the matrix-element level before parton showering is invoked.

To accurately simulate high-p_T events and to account for configurations with more than one hard parton inside a large jet, we employ SHERPA's matrix-element–parton-shower matching algorithm [70, 71]. We consider the complete sets of tree-level matrix elements with up to two (four) additional final-state partons for $t\bar{t}$ and dijet (W/Z) production from SHERPA's matrix-element generator COMIX [72]. The matrix elements of varying multiplicity are consistently combined to form inclusive samples of fully exclusive events through subsequent parton shower evolution [73] before being subjected to hadronization. The renormalization and factorization scales are dynamically determined on an event-by-event basis according to the matching algorithm [70]. For the parton separation parameter of the matching procedure we use $Q_{\text{cut}} = 20$ GeV. The default tune of SHERPA 1.3.1 for the hadronization and underlying event model parameters was used.

5.1.2. HERWIG++ *events* For comparison with last year's HERWIG events we have also produced samples using HERWIG++ 2.5.0. The initial state consists of two beams of protons at a centre-of-mass energy of 7 TeV. The underlying event has been simulated using the UE7-2 tune, whose parameters can be found at http://projects.hepforge.org/~herwig/MB_UE_tunes/input_cards/LHC-UE7-2.in. The samples have been produced using Standard Model matrix elements for QCD $2 \rightarrow 2$ scattering and $t\bar{t}$ production. Only fully hadronic final states are considered. For each process 10,000 events were produced for each p_T bin of a width of 100 GeV, from 200

∗We omit other possibilities only for reasons of time and space, and not any stance on the superiority of particular programs.

GeV to 800 GeV for $t\bar{t}$ production and from 200 GeV to 1.6 TeV for QCD $2 \rightarrow 2$ scattering. The resulting p_T distribution when combining all samples is approximately flat. The p_T cut is applied at the level of the hard process. B hadrons have been set stable through a lifetime cut of 1 ps, for consistency with the HERWIG samples used for BOOST 2010.∗ All other settings have been left as default.

5.2. New tools

The BOOST 2010 report compared the Johns Hopkins top tagger [31], its CMS variant [32], an ATLAS tagger based on k_T scales [74], the so-called "Thaler and Wang" tagger based on a similar kinematic variable z_{cell} [75], and a tagger using pruned jet and subjet masses [33, 34]. Detailed descriptions of these taggers may be found in the 2010 report [1]. To this list we add a trimming-based tagger [65] as well as the HEP and N-subjettiness taggers described in Section 3.

The HEP tagger used in this section is a somewhat different implementation than the one described in Section 3, essentially corresponding to the tagger described in [44].† Rather than apply the subjet mass criteria of [60] we simply identify the W as the pair of the three identified subjets with mass closest to m_W, and measure its mass and helicity angle as in the JH and CMS taggers. Both schemes make use of the mass and decay kinematics of the $t \rightarrow Wb \rightarrow q\bar{q}b$ system, so after optimising parameters and measurement cuts it is not clear how much of an improvement the new symmetric mass cuts give. We leave this question, just as possible optimisations of the tagging cuts [62], to detailed joint experimental and theoretical studies.

For the N-subjettiness tagger we find subjet axes via "one-pass minimisation" of k_T axes. That is, three subjets are identified via the exclusive k_T algorithm, then a single iteration of the minimisation procedure described in [56] is applied. The parameter β is set to 1.0.

5.3. General analysis description

As for the 2010 report, all analyses begin with anti-k_T jets with $R = 1.0$, $p_T > 200$ GeV.‡ For the Hopkins, CMS, HEP, and trimmed taggers, jets are first reclustered with Cambridge-Aachen, which is also the algorithm used in the pruning stage of the pruned analysis. For the ATLAS and Thaler and Wang taggers jets are reclustered with k_T before measuring substructure. N-subjettiness is a jet shape, so no reclustering is necessary.

For each tagger, we identify the set of input parameters to be tuned as well as the set of output variables to cut on. These are given in Table 1. The Hopkins, CMS, and HEP

∗During final preparation of this report, we discovered that due to an apparent bug in Herwig++ 2.5.0, B^0 hadrons can still decay through mixing.

†Specifically, we use version 1.0 of the `HepTopTagger.hh` code provided by the tagger authors, and have defined "passing" as the result of the `is_maybe_top()` function instead of `is_masscut_passed()`.

‡It would of course be interesting to see what could be accomplished with smaller or larger R values, especially larger R at lower p_T, but we do not consider this possibility here.

taggers all have a built-in method of identifying the W subjet. For fairness, in the other taggers we include a W-identifying step: the jet (after grooming for pruning/trimming) is unclustered to three subjets and the pair with the minimum pairwise mass is merged to form the W. This mimics the W-finding step in the CMS tagger.

Analysis	Input parameters	Output variables
ATLAS	N/A	$\left\{m_J^0, m_W^{k_T}, z_{\mathrm{cut}}^1, z_{\mathrm{cut}}^2\right\}$
CMS	$\{\delta_p, \delta_r\}$	$\{m_J^0, m_W, \cos\theta_h\}$
Johns Hopkins	$\{\delta_p, \delta_r\}$	$\{m_J, m_W, \cos\theta_h\}$
HEP	$\left\{\mu, m_{\mathrm{subjet}}^{\max}\right\}$	$\{m_J, m_W, \cos\theta_h\}$
N-subjettiness	N/A	$\{m_J^0, \tau_3/\tau_2\}$
Pruning	$\{z_{\mathrm{cut}}, R_{\mathrm{cut}}\}$	$\{m_J, m_W\}$
Thaler and Wang	N/A	$\left\{m_J^0, m_W^{k_T}, z_{\mathrm{cell}}\right\}$
Trimming	$\left\{R_{\mathrm{sub}}, p_T^{\mathrm{frac}}\right\}$	$\{m_J, m_W\}$

Table 1. Input parameters and output variables for each top tagging analysis. m_J^0 is the jet mass found by the original algorithm; m_J is after any substructure modification. For the HEP tagger, μ is the mass drop threshold and $m_{\mathrm{subjet}}^{\max}$ is the subjet mass where declustering stops.

The optimal output cuts for any given input variables and signal efficiency are found using TMVA [76]; input variables are scanned with a Python script and the lowest mistag rate is kept for each bin in signal efficiency. To avoid pathological optimisations where TMVA finds W jets instead of top jets, we require that the jet mass cut have a lower bound of at least 120 GeV. The statistical noise from fluctuations in the testing and training samples is significant, so in each efficiency plot a five-point moving average is applied.

One might not always want to re-optimise the input parameters of a tagger for each p_T range, signal efficiency, etc. To give a sense of how well each tagger performs without scanning its parameters, we repeat the efficiency scans with a single set of input parameters. For each Monte Carlo sample, we take the parameters found at the 35% signal efficiency point, in the 500–600 GeV p_T bin, as this common point. These parameters are given in Table 2.

The analyses are implemented in SpartyJet [77, 78], using tools based on FastJet [79, 66]. All are available either as internal FastJet tools in version 3.0.0 or as add-ons available on the FastJet tools site at http://fastjet.fr/tools.html. The Python scripts used to define the analyses, perform the efficiency scans, and make the plots, along with instructions, can be found on the BOOST 2011 website, http://boost2011.org.

	Input parameters		
Analysis	HERWIG 6.5	HERWIG++	SHERPA
CMS	$\{\delta_p, \delta_r\} = \{0.028,\, 0.13\}$	$\{0.028,\, 0.20\}$	$\{0.056,\, 0.47\}$
HEP	$\left\{\mu, m_{\mathrm{subjet}}^{\max}\right\} = \{0.93,\, 54\}$	$\{1.0,\, 46\}$	$\{0.87,\, 10\}$
Johns Hopkins	$\{\delta_p, \delta_r\} = \{0.083,\, 0.19\}$	$\{0.056,\, 0.23\}$	$\{0.083,\, 0.27\}$
Pruning	$\{z_{\mathrm{cut}}, R_{\mathrm{cut}}\} = \{0.056,\, 0.33\}$	$\{0.056,\, 0.33\}$	$\{0.056,\, 0.22\}$
Trimming	$\left\{p_T^{\mathrm{frac}}, R_{\mathrm{sub}}\right\} = \{0.050,\, 0.19\}$	$\{0.050,\, 0.28\}$	$\{0.083,\, 0.28\}$

Table 2. Input parameters for each tagger, found by scanning over reasonable values and taking the lowest mis-tag rate for a 35% signal efficiency, in the 500–600 GeV p_T bin. These parameters are then used in all plots where input parameters are *not* varied. The ATLAS, N-subjettiness, and Thaler and Wang taggers are not shown as they do not have input parameters.

5.4. Results

We begin with a simple extension of the 2010 results (Figure 3 in [1]). In Figure 14 we show mis-tag vs. efficiency curves for the expanded set of top taggers, as tested on last year's HERWIG 6.5 samples. We can see that the groomed taggers (pruning and trimming plus mass cuts), "hybrid" taggers that incorporate grooming as well as measurement (CMS, HEP, JH), and the N-subjettiness jet shape, outperform the ATLAS and Thaler and Wang taggers, which use subjet measurements exclusively. The groomed, hybrid, and jet shape taggers are comparable in performance, with the groomed and N-subjettiness taggers performing best at low signal efficiency. In the lower set of plots, where we do not scan over input parameters, N-subjettiness performs noticeably better over most of the efficiency range.

To complement the HERWIG 6.5 samples from last year, we have generated equivalent samples in HERWIG++ as a cross-check. The results are shown in Figure 15. The results are broadly similar to those for HERWIG 6.5, but the spread between different methods is reduced. With or without input optimisation, there is no clear "winner".

Both Monte Carlo samples used last year were generated via $2 \rightarrow 2$ processes interfaced with a parton shower; this year we add matched samples from SHERPA to explore the effects of adding higher-order matrix elements. We expect that these higher-order effects should lead to a more precise description of the hard, wide-angle radiation that forms the most challenging background to heavy particle jets.

In Figure 16 we repeat the analyses of Figure 14 on matched samples from SHERPA. The p_T cuts are the same. Comparing to Figure 14 we see that the different multijet modelling predicts substantially worse performance for all taggers, presumably due to enhanced hard substructure in the background. The relative performance of different taggers, though, is similar to the unmatched samples. Other than ATLAS and Thaler and Wang, which continue to be less effective, the taggers are extremely
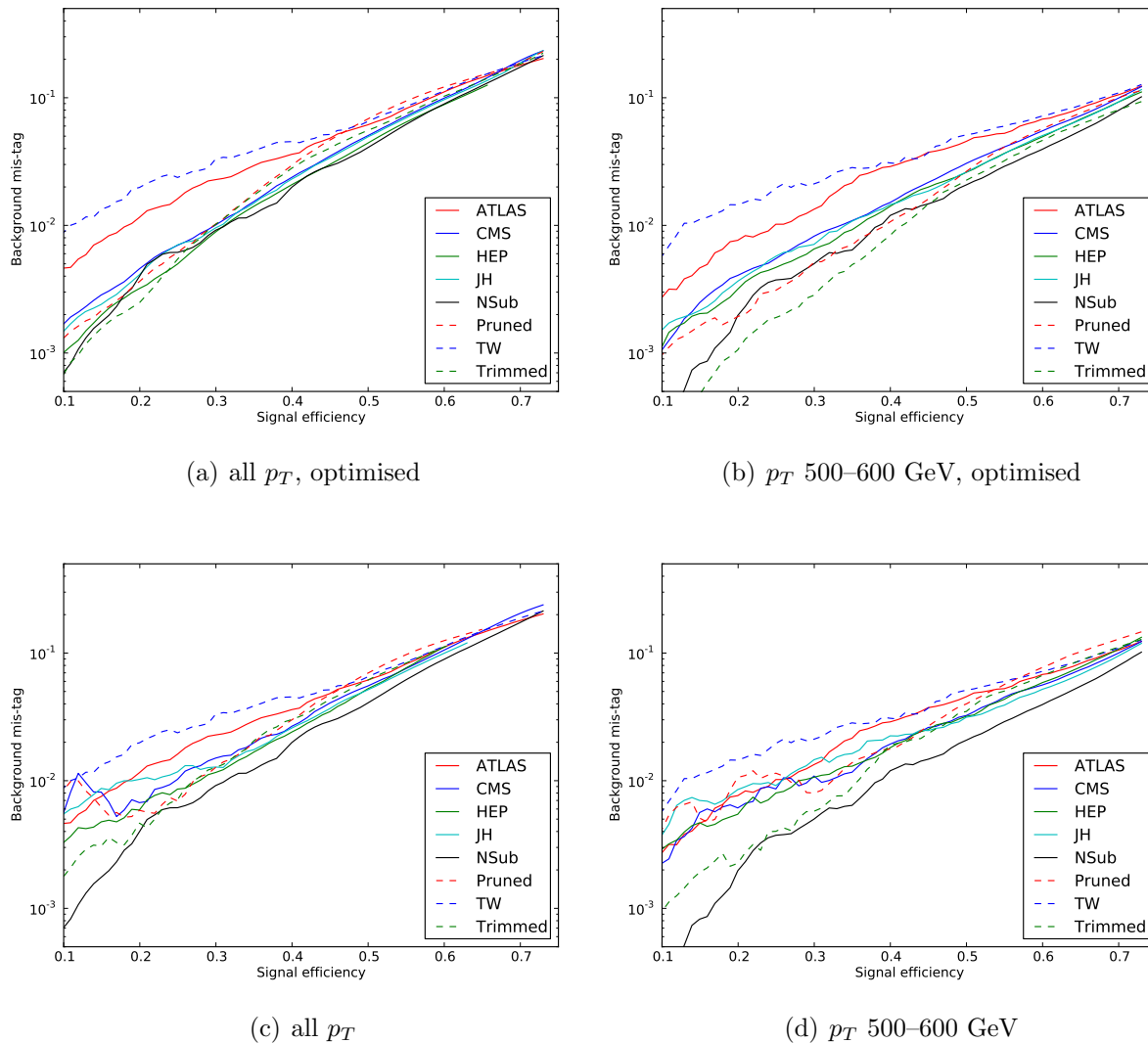
(a) all p_T, optimised

(b) p_T 500–600 GeV, optimised

(c) all p_T

(d) p_T 500–600 GeV

Figure 14. Mis-tag vs. efficiency for several top tagging methods, as tested on HERWIG 6.5 $t\bar{t}$ and dijet samples. For Figures (a) and (b), the input parameters are optimised for each efficiency point. The input parameters for the unoptimised scans are taken from the 35% efficiency point in Figure (b).

similar in performance. When we do not scan input parameters, N-subjettiness narrowly outperforms the hybrid taggers.

The plots thus far represent events with no detector simulation. How do the results change if we add detector resolution effects? In Figure 17, we repeat the analyses, but acting on events run through a simple calorimeter simulation provided by Peter Loch, presented at the BOOST workshop. This simulation smears energy according to a radial profile based on performance of the ATLAS detector, then groups energy deposits into calorimeter cells. Each calorimeter cell is then treated as a massless particle with the direction and total energy of that cell. The resulting events provide a crude proxy for the real calorimeter output and give us a way to estimate detector effects on substructure
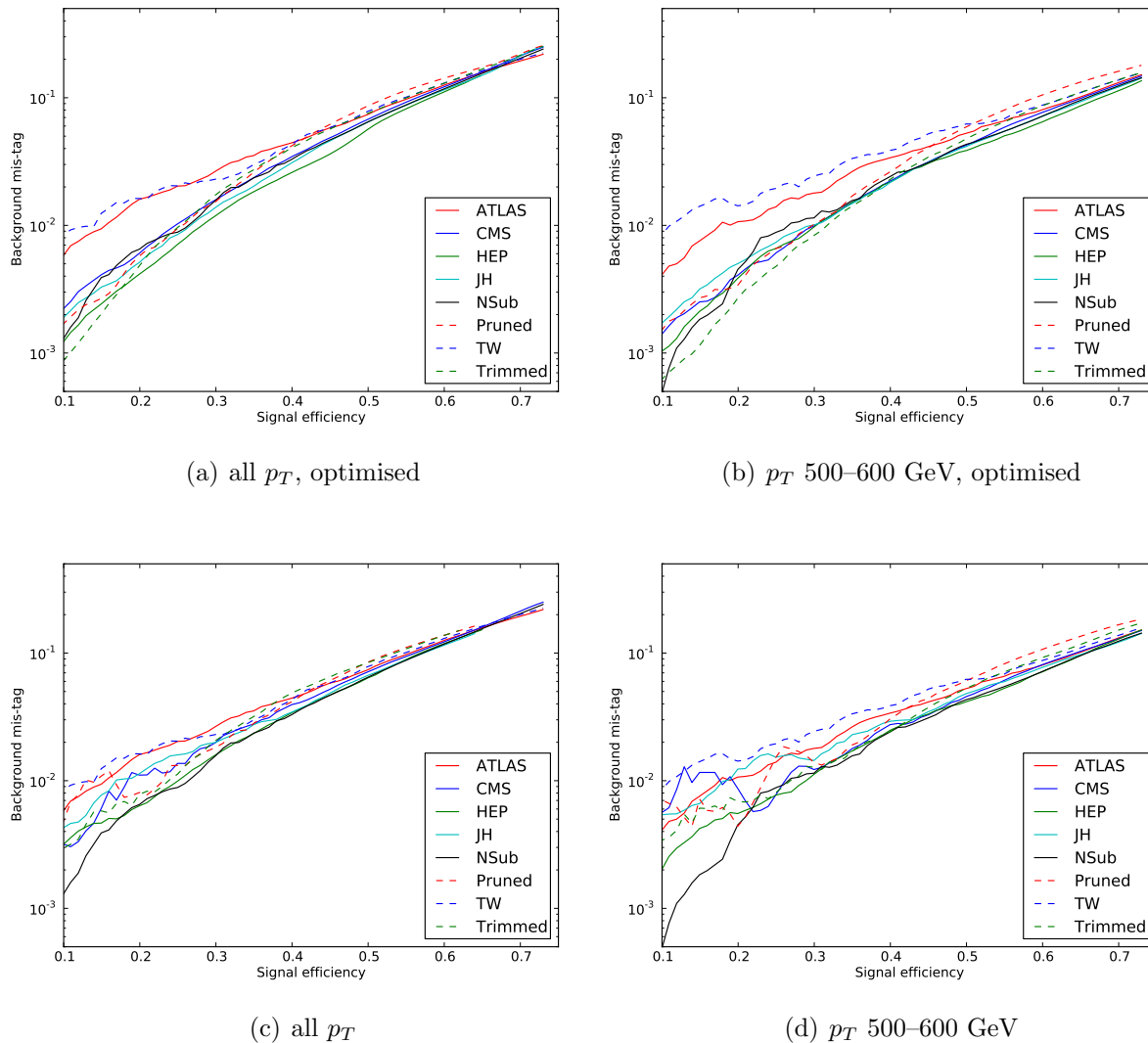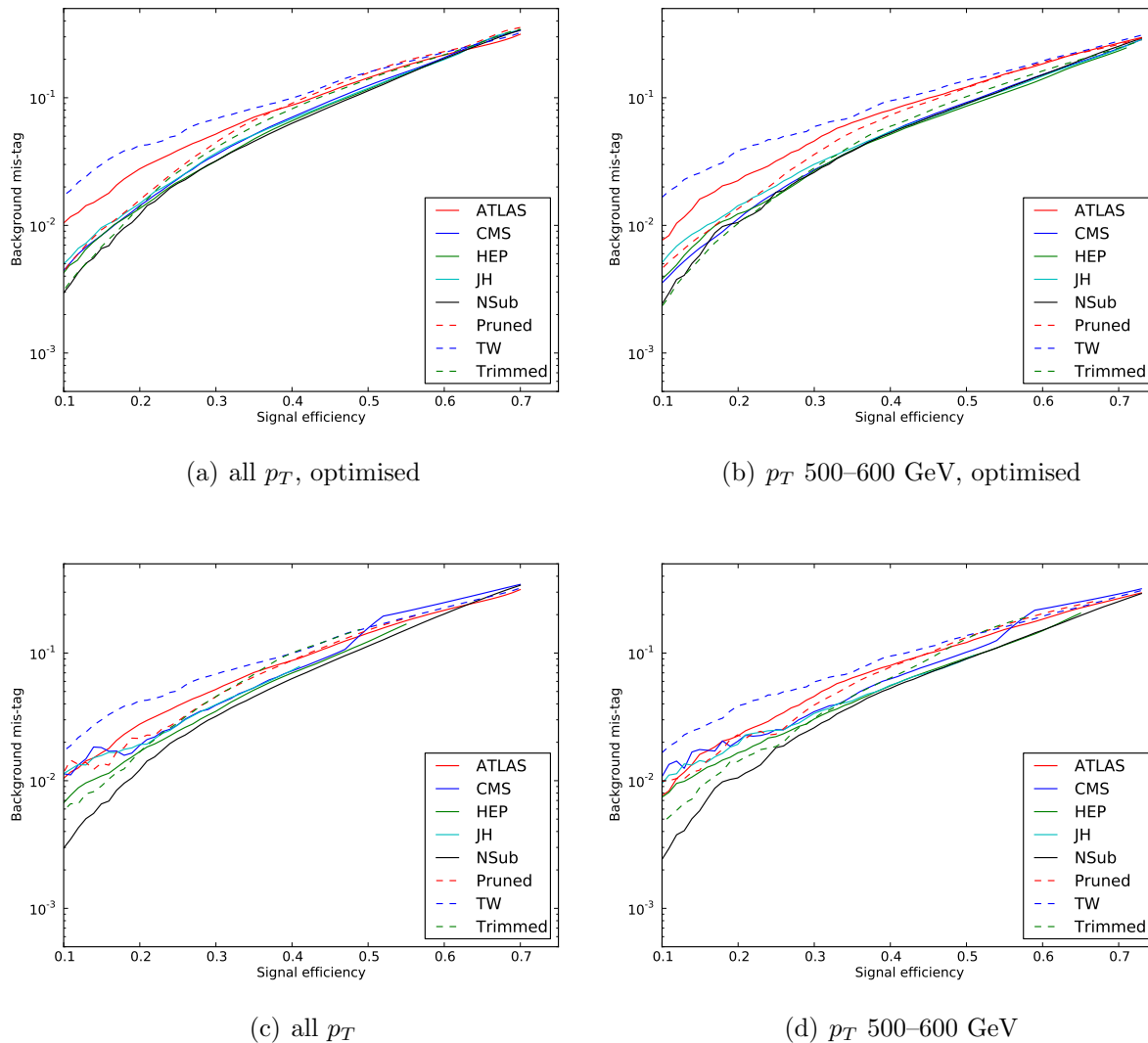
(a) all p_T, optimised

(b) p_T 500–600 GeV, optimised

(c) all p_T

(d) p_T 500–600 GeV

Figure 15. Mis-tag vs. efficiency for several top tagging methods, as tested on HERWIG++ $t\bar{t}$ and dijet samples. For Figures (a) and (b), the input parameters are optimised for each efficiency point. The input parameters for the unoptimised scans are taken from the 35% efficiency point in Figure (b).

performance. This simulation has yet to be extensively studied, so the results presented here should be considered preliminary and interpreted with caution.

The detector simulation code is available at the author's website, http://atlas.physics.arizona.edu/~loch, and is also provided with SpartyJet as the `RadialSmearingTool` tool. You can use it in a SpartyJet analysis via:

```
builder = SJ.JetBuilder()
builder.add_jetTool_input(SJ.RadialSmearingTool())

<add analyses and run...>
```

Comparing Figures 14–16 with 17 we can see that including realistic detector
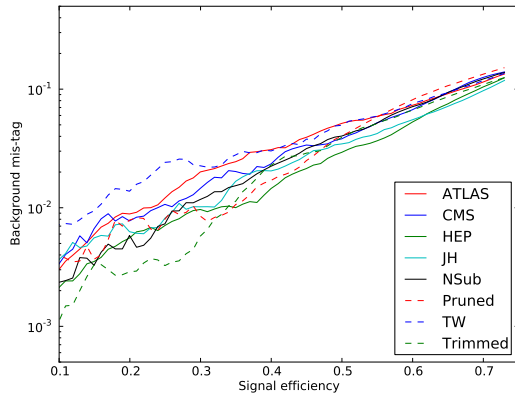
(a) all p_T, optimised

(b) p_T 500–600 GeV, optimised
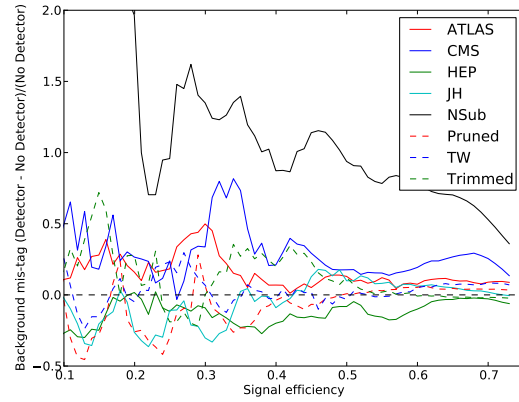
(c) all p_T

(d) p_T 500–600 GeV

Figure 16. Mis-tag vs. efficiency for several top tagging methods, as tested on SHERPA matched $t\bar{t}+$ jets and multijet samples. For Figures (a) and (b), the input parameters are optimised for each efficiency point. The input parameters for the unoptimised scans are taken from the 35% efficiency point in Figure (b).

resolution generally degrades the best achievable performance and changes how algorithms compare to each other. Compared to other taggers, N-subjettiness does worse. For each MC sample the spread between taggers is still small, with the ATLAS and Thaler and Wang taggers still being outperformed. Considering the right-hand plots in Figure 17, we can see that in some cases taggers appear to do better after detector simulation, especially at low signal efficiency. This effect is at least partly due to statistical noise in the efficiency scans, but warrants further study.
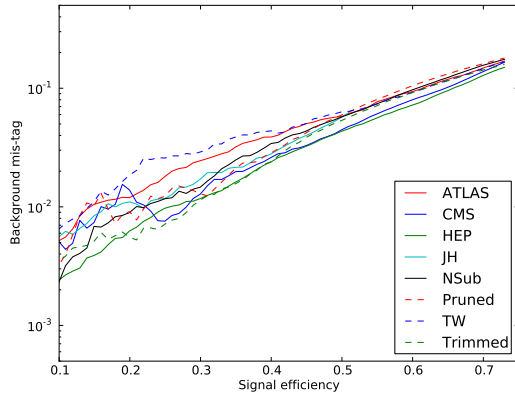
The results we have presented in this report, while certainly not providing the last word in boosted object tagging, suggest some conclusions. By any metric, methods that use only subjet kinematic information, like the ATLAS and Thaler and Wang
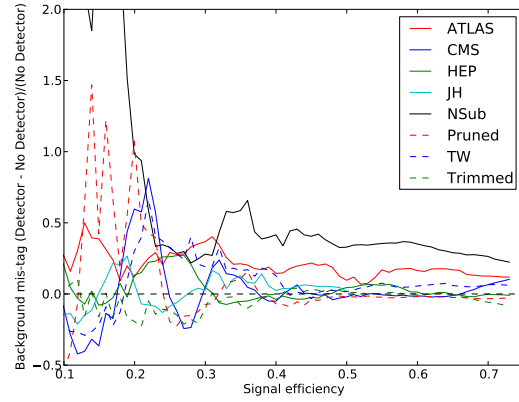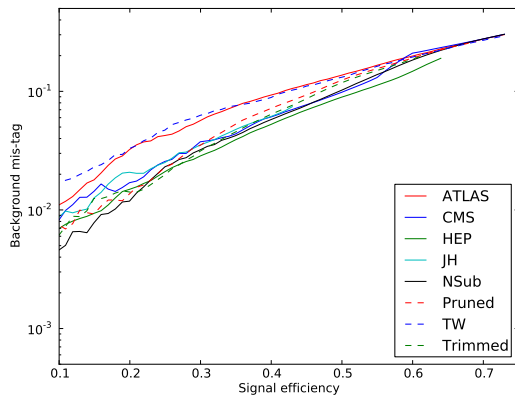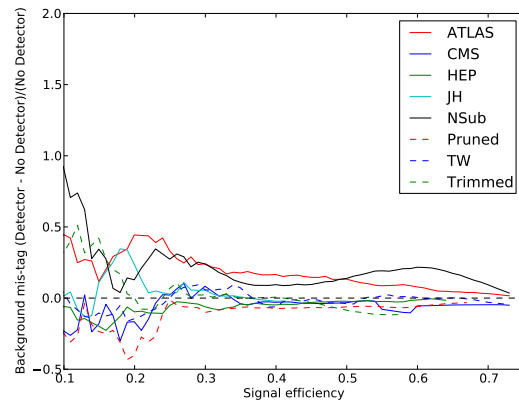
(a) HERWIG

(b) HERWIG, fractional difference

(c) HERWIG++

(d) HERWIG++, fractional difference

(e) SHERPA

(f) SHERPA, fractional difference

Figure 17. Mis-tag vs. efficiency for several top tagging methods, as tested on HERWIG 6.5 and HERWIG++ $t\bar{t}$ and dijet samples as well as SHERPA matched $t\bar{t}$ + jets and multijet samples, all with p_T 500–600 GeV. Events have been run through a simple detector simulation. In the right-hand plots, results after detector simulation are compared with results before simulation; the y axis is $(\epsilon_B(\text{detector}) - \epsilon_B(\text{no detector}))/\epsilon_B(\text{no detector})$. All plots use the input parameters in Table 2.

taggers, are outperformed by groomed, hybrid, and jet shape taggers. Differences between the rest of the taggers are largely of similar magnitude to differences between Monte Carlo samples and before and after detector simulation: more careful study would be needed to definitively say that some are better than others. In these studies, the N-subjettiness tagger does particularly well when compared to other taggers with fixed input parameters, but when optimisation is included performances are extremely similar. N-subjettiness also appears to be particularly susceptible to degradation due to detector resolution.

Beyond the limited comparisons given in this section, we hope that the software tools we have developed to make them will facilitate further study. Such study is clearly warranted to seriously answer the questions posed at the beginning of this section. Further phenomenological exploration of the broad space of substructure techniques will help lead to a more holistic understanding of substructure physics. Monte Carlo study will complement developments in jet calculations, a subject to which we now turn.

6. What is calculable and measurable in 2012?

Since the start of the LHC physics program, the ATLAS and CMS experiments have made substantial progress in measuring jet properties. Interest in using jet properties for new physics searches has placed a large emphasis on understanding jets more thoroughly than at previous experiments. The improved resolution of the detectors has made this possible, and current progress is very promising for the future of jet physics in the age of the LHC. This has naturally excited the interest of the theory community, whose continued work on jet physics will confront data in the coming years. This section is devoted to a summary of theoretical work related to jet substructure, focusing on observables whose properties can be calculated and measured in the near term.

Two complementary tools are used to understand jet properties: analytic calculation and Monte Carlo simulation. Analytic calculations give an inclusive picture of a jet or event, often projecting onto single observables. MC generators offer totally exclusive events, on which any number of observables can be measured. These programs can simulate effects that are challenging to integrate into a calculation, such as the underlying event, pile-up, and hadronisation. State-of-the-art calculations have perturbative precision that often exceeds MC generators (either in fixed order or resummed terms), but these calculations are only feasible for a limited set of observables. Importantly, improvements in analytic calculations help further development and validation of MC generators. Improvements in calculations will also play a key role in interpreting jet measurements at the LHC.

Calculations of jet properties typically focus on single jet observables, also known as jet shapes. These variables are inclusive over the jet constituents, measuring a function of the final state momenta. By contrast, most jet substructure methods involve more complicated partitioning of the jet constituents and observables of localised structure in the jet. While many early studies used subjet information to identify the hadronic decays

of heavy particles, recent studies have explored the efficacy of jet shapes in boosted heavy object searches (e.g., [38, 41]). Observables derived from the N-subjettiness jet shapes have been shown to be very competitive in top tagging (see also Section 5). This gives hope that calculationally simpler observables may be useful in new physics searches.

In this section we will discuss the calculation of jet observables, focusing on jet mass, which provides an example of a jet observable that can be usefully calculated. We present aspects of the calculation and discuss improvements that can be made with future work. We then discuss other observables that are useful for measurement and point out where calculations may soon be available.

6.1. Jet mass as an example

Jet mass is the simplest and most phenomenologically useful jet shape. An accurate measurement depends on a good understanding of the jet energy scale and splash-in contributions (pile-up, the underlying event, and initial state radiation). The importance of the measurement and the accessibility of the calculation mean that a comparison between the two can be very useful.

The measurement of a single jet mass is still a complex observable. The calculation is performed for an exclusive jet multiplicity, meaning there must be a veto on additional jets. Consider the cross section for dijet events from the anti-k_T algorithm, differential in both jet masses, $d^2\sigma/dm_1 dm_2$. We must veto on additional jets by placing a p_T cut on candidate jets found by the algorithm. Additionally, the perturbative calculation is only valid for high-p_T jets, meaning a restriction of the phase space for the hard scattering is required.

There are two main regimes in the jet mass distribution. The small mass regime, $m_J \ll p_{TJ}$, contains large logs of m_J/p_{TJ}. Resummation is required to tame these large logs and restore accuracy. For larger masses, a fixed order calculation suffices to describe the distribution. Next-to-leading order is currently state-of-the-art for a wide range of processes, and can be simulated by Monte Carlo for many processes.

The small jet mass limit is the focus of the most effort in the calculation. Resummation must be performed in this regime, which requires proving certain properties of the cross section. In particular, some kind of factorisation must be proven that relates the all-orders, large-log terms to the fixed order terms.

The additional factorisation required for resummation of jet mass takes two basic forms, depending on what tools are used. Both perturbative QCD and soft-collinear effective theory (SCET) can be used to resum the jet mass distribution, and the essential physics that each uses is the same. However, the language each uses is distinct, and a comparison of them would be useful. Here we give an outline of factorisation in SCET; some features of resummation in SCET and QCD are compared in the next subsection.

In the SCET formulation of the cross section, an effective theory framework is used [80, 81, 82, 83]. Hard modes that produce perturbative emissions of energetic partons are integrated out of QCD. The remaining soft and collinear modes have momenta

parameterised by a power counting parameter $\lambda \ll 1$. This power counting parameter is typically determined by the kinematics of the final state; for the jet mass example, $\lambda = m_J/p_{TJ}$. The soft and collinear fields decouple at leading power in the SCET Lagrangian [83], decoupling the N-jet operators used to describe the energetic jets. Factorisation also requires showing that the measurement (such as the jet mass with the anti-k_T algorithm and a p_T cut on additional jets) factorizes as well. This means the phase space constraints on soft and collinear modes must separate. This can be shown formally by providing an operator formulation of the phase space constraints [84, 85], and can also be seen at a physical level by a power counting analysis of the measurement in terms of the modes in SCET [86]. This leads to a schematic factorisation theorem of the form, for N jets:

$$\sigma = H_N \left[B_a \times B_b \times J_1 \times \cdots \times J_N \right] \otimes S_N \,. \tag{10}$$

The hard function H_N is the matching coefficient onto SCET and arises from the short-distance interaction that produces the well-separated, energetic partons. The jet functions J_i and beam functions $B_{a,b}$ come from the final and initial state collinear evolution of the hard partons [87]. The soft function S_N comes from the global soft gluon radiation across the event. Each of these functions can be separately calculated in perturbation theory, and renormalisation group evolution is used to sum the large logarithms that arise in the cross section. This framework formalises much of the resummation machinery used in perturbative QCD.

6.1.1. Facets of the calculation We first discuss the perturbative contributions to the cross section, in particular the resummation. We focus on jets in the anti-k_T algorithm, since jets defined in other algorithms are complicated by the non-trivial role of clustering between soft gluons. Soft gluon clustering in these algorithms means that the soft phase space does not factorize into single particle phase space for each soft gluon, affecting the subleading logarithms in the perturbative series starting at $\mathcal{O}(\alpha_s^2 \ln^2)$ [88, 89]. In the anti-k_T algorithm the phase space for a single soft particle is not affected by the presence of other soft particles.

The leading logs in the cross section are given by the exponentiation of single soft gluon emission in QCD, and single-log and running-coupling corrections can be included. Equivalently in SCET, the leading logs are specified by the cusp anomalous dimensions of the one-loop jet and soft functions, with the single-log terms coming from the non-cusp anomalous dimensions. Running-coupling effects arise in renormalisation group evolution. In the limit of small jet radius ($R \ll 1$), the leading logs have the form

$$\int_0^m \frac{\mathrm{d}\sigma}{\mathrm{d}m} \sim \sigma_0 \exp \left(-\frac{\alpha_s C_F}{2\pi} \ln^2 \frac{m}{p_T R^2} \right) . \tag{11}$$

In principle, subleading logarithms can be straightforwardly computed and resummed. The extension of resummation techniques beyond next-to-leading-log (NLL) is natural using the SCET framework. However, general jet shapes suffer from non-global

logarithms that contribute at NLL [90]. Nearly every jet measurement made at the LHC will have non-global observables, and their resummation is more challenging and can only be performed in the leading-colour approximation [90, 91, 92, 93]. The physics of the leading non-global logs at fixed order (α_s^2) has been well understood in QCD, and their resummation calculated numerically in the large-N_C limit. Recent explorations in SCET have provided additional insights into their structure and origin, providing a possible new path to renormalisation group-based resummation [94, 95, 96]. Non-global logs are reduced by soft gluon clustering, and so are reduced for algorithms other than anti-k_T [91, 96].

The small-R approximation is advantageous because a simple picture of non-global logs emerges. Each jet has its own non-global correction factor, and cross talk between jets is relegated to a power-suppressed contribution in R. The non-global factor for a jet was calculated in the large-N_c limit in [90] and used for jet mass in [93]. The large-N_c approximation will receive corrections from subleading colour terms which will modify the non-global log contribution at around the ten percent level. Since non-global logs contribute at NLL and start at $\mathcal{O}(\alpha_s^2 \ln^2)$, subleading terms in colour ought not to matter phenomenologically, as was the case for deep inelastic scattering event shapes [97]. Thus in the small-R approximation the cross section is described by a resummed factor for each jet dressed by a calculated non-global factor, and one can include jet mass measurements for each jet [93].

Beyond the small-R approximation, one can account for the corrections by including terms that vanish as powers of R. In QCD, one computes soft gluon emission from all of the colour dipoles in the event, including the incoming partons. Expanding the result as a power series in R, one finds that the terms of relative order R^2 make a numerical impact (at around the ten percent level even for $R = 0.4$), but terms scaling as R^4 do not matter even for $R = 1$. Similarly, the non-global factor must be corrected beyond the small-R limit. In SCET, the sum over soft gluon emission from colour dipoles is given in the soft function, where one expands in

$$t_{ij}^{-1} \equiv \frac{\tan^2 R/2}{\tan^2 \theta_{ij}/2} \,, \tag{12}$$

with θ_{ij} the angle between jets i and j [98, 54]. The requirement $1/t_{ij} \ll 1$ forces the jets to be well-separated, which is needed to factorize the cross section. When jets become close together, additional modes in SCET are required to separate the scale dependence on the small dijet invariant mass [99]. These modes parameterize soft radiation between the nearby jets, and SCET can be formally extended to SCET$_+$, which includes these modes.

Therefore, for a wide range of jet mass measurements it should be possible to obtain a resummed result that accounts for non-global logarithms and goes beyond the small-R approximation to sufficient accuracy so as to be phenomenologically useful.

A resummed calculation describes the dominant shape of the distribution. However, many other effects must be taken into account. The shape of the large-mass tail of

the distribution is described well by fixed-order QCD. The resummed and fixed-order calculations can be combined in a simple way:

$$\frac{\mathrm{d}\sigma}{\mathrm{d}m} = \left.\frac{\mathrm{d}\sigma}{\mathrm{d}m}\right|_{\mathrm{resum}} - \left.\frac{\mathrm{d}\sigma}{\mathrm{d}m}\right|_{\mathrm{resum}}^{\mathrm{FO\ exp}} + \left.\frac{\mathrm{d}\sigma}{\mathrm{d}m}\right|_{\mathrm{FO}}. \tag{13}$$

The resummed and fixed order distributions are added, and the fixed order expansion of the resummed distribution is subtracted. In the small-mass limit, the two fixed order functions cancel up to power corrections in m/p_T, and the resummed distribution correctly describes the distribution. In the large-mass tail, the resummed distributions (all orders and fixed-order expanded) cancel up to the fixed order in α_s of the expansion, so the fixed-order QCD distribution describes the shape up to higher-order corrections.

Hadronisation, pile-up, and underlying event contributions must also be included in a calculation of the jet mass. These non-perturbative contributions affect the small-mass regime of the distribution, and are needed for the calculation to be compared to data. While important, these effects are challenging to include, as no framework exists to systemically include them and they require a more detailed understanding of the data.

Basic models have been formulated to quantify contributions from the underlying event and pile-up [100, 14, 6, 101]. As jet shapes are measured and calculated more extensively, the comparison between the two is a good testing ground to study these models and fold them into calculations. In the case of 2-jet event shapes in e^+e^- collisions, the correction to the first moment of the event shape from non-perturbative effects has been shown to be related to a universal, measurable non-perturbative matrix element for a wide class of event shapes [102, 103]. In the SCET framework, model soft functions that parameterise non-perturbative effects have also been introduced [104]. Further study is warranted to understand the how non-perturbative effects in a hadron collider environment can be introduced, and whether similar universality relations that exist in e^+e^- collisions apply in the hadron collider case.

6.2. Measurable and calculable observables

A wide array of observables have been defined to study the structure of jets. While the jet mass is phenomenologically the most important, it is important to prioritise which other observables should be measured in the near term at the LHC. There are several key reasons to measure jet substructure. The comparison to precision QCD calculations is obviously attractive, and understanding QCD backgrounds helps characterise observables relevant for new physics searches. Additionally, jet substructure measurements can further understanding of detector effects and improve unfolding techniques. This can have an impact beyond jet substructure measurements, such as a reduction in the jet energy scale uncertainty.

There are four general classes of observables used to measure jet substructure and jetty events:

- Jet mass
- Jet shapes
- Groomed jet observables
- Global event shapes

Although jet mass is a jet shape, it is central enough to jet physics that special consideration should be given to it as a first measurement. Jet grooming methods are generic substructure methods that remove isolated soft radiation in jets. Three grooming methods have been proposed: filtering [35], pruning [33], and trimming [65]. The measurement of properties of groomed jets can provide data about the structure of the jet that is difficult to capture with simpler observables such as jet shapes. Finally, global event shapes can be measured without clustering into jets. Several event shapes are useful in characterising soft physics that can contribute to jet substructure.

Below we discuss each class of observables, identifying key observables in each category. These are measurements that theorists find informative, and will help in the study of jet substructure. Many of these observables may be calculated in the near term, and measurement of them can provide motivation for a detailed comparison.

6.2.1. Jet mass measurements There are several possible channels in which a jet mass distribution can be measured. These include pure QCD events with inclusive and exclusive jet cross sections, jets produced in association with electroweak bosons, and light quark jets produced in association with top quarks. Because the calculation of a jet mass distribution depends on the precise event topologies studied, to compare theory and experiment it is important to carefully choose the measurements. Several key topologies will provide important jet mass measurements. The three we focus on are $\gamma/W/Z$ + jet, dijet, and multijet events. In each topology, there are particular jet mass observables of interest, specialised to the final state.

- **$\gamma/\mathbf{W}/\mathbf{Z}$ + jet events** – These have only a single jet in the final state (assuming the W or Z decays leptonically) and provide the cleanest jet measurements. This class of events is an important reference sample for jet energy scale calibration, and can be used to measure fake rates for certain substructure tagging algorithms. They are a source of jet + lepton and jet + MET final states, and are a background to many new physics searches. Theoretically, they can be used as precision tests of QCD and provide a more calculable environment due to the single jet multiplicity. The observable of interest is the differential jet mass distribution, $\mathrm{d}\sigma/\mathrm{d}m_J$, in bins of jet p_T. A jet veto must be imposed to obtain an exclusive sample of single jet events. A hard veto on additional jets, such as $p_{T_J} < 0.1\, p_T^\gamma$, can be useful for jet energy scale calibration. The jet mass distribution in this case is of interest because of the restriction on radiation outside the singe jet. For any value of the jet veto, if the jet mass distribution is finely binned in p_T (several bins instead of one or two), the impact of various components of the calculation can be compared across p_T.

- **dijet events** – Dijet events with high-p_T jets have a large cross section and make up a significant fraction of the pure QCD events containing high-p_T jets at the LHC. These events are backgrounds to many new physics searches, and their large cross section means that they must be precisely understood.

  Because there are multiple jets in the event, different jet mass measurements can be made. The doubly differential distribution,

  $$\frac{\mathrm{d}^2\sigma}{\mathrm{d}m_1\mathrm{d}m_2}, \tag{14}$$

  with $p_{T1} > p_{T2}$, is interesting because correlations between the jet masses can be studied. This was explored in the CDF analysis of jet mass [105], where the ratio of event numbers in different bins in the double differential distribution was measured. Define two single-jet mass bins b_1 and b_2 (in the CDF study $b_1 = (30, 50)$ GeV and $b_2 = (130, 210)$ GeV). These bins define four regions:

  $$
  \begin{aligned}
  A &: m_1 \in b_1, \quad m_2 \in b_1, \\
  B &: m_1 \in b_2, \quad m_2 \in b_1, \\
  C &: m_1 \in b_1, \quad m_2 \in b_2, \\
  D &: m_1 \in b_2, \quad m_2 \in b_2.
  \end{aligned} \tag{15}
  $$

  $$\tag{16}$$

  Then define the ratio R_{mass} to be

  $$R_{\mathrm{mass}} \equiv \frac{N_B N_C}{N_A N_D}. \tag{17}$$

  If the jet mass distributions were independent, then $R_{\mathrm{mass}} = 1$. Correlations between these distribution exist because of soft gluon exchange, although the expected value of R is not known. This observable is of interest due to the discrepancy between Monte Carlo simulation and data, and a theory calculation could help resolve the differences.

  In addition to the doubly differential mass distribution, the projection onto a single mass is theoretically accessible. Common choices are the heavy jet mass and the sum of jet masses, which have been studied at e^+e^- colliders. The hardest jet's mass is harder to predict theoretically because the relative p_T in dijet events is affected primarily by soft physics.

- **multijet events** – Events with more than two jets provide a more complex background. The colour correlations between jets are enhanced as the detector becomes more crowded, and these events typically have a hierarchy of jet p_T's. Multijet events are more important at the LHC due to the increased phase space for high-p_T parton production, and significant attention has been paid to understanding them better theoretically and experimentally. Multijet events present a theoretical challenge to describe, but also offer the opportunity to learn about effects such as colour correlations that figure less prominently in simpler events.

In multijet events, placing a hard p_T cut on the leading three jets will give a multijet event sample that allows one to study the structure of the hardest jet as the kinematics of the events change. In particular, the jet mass distribution of the hardest jet can be measured in bins of the ΔR separation to the nearest jet. As jets become closer together, inter-jet soft radiation can have a large effect on the mass distribution. This can be predicted theoretically, and the result compared with the Monte Carlo.

Because the jet mass is sensitive to the environment of the event, it is important to examine the effect of event-wide characteristics on the mass. As pile-up increases, the jet mass can serve as a probe of the size of the pile-up and the effectiveness of subtraction methods (see Section 2.3.1).

The rapidities of the hard jets will affect the jet mass distribution, for a number of reasons. First, large-rapidity jets imply a large momentum asymmetry between the initial partons, meaning that one carries a large fraction of the proton momentum ($x \sim 0.1$). Since the quark parton distribution functions dominate in this regime, the fraction of quark jets will be enhanced relative to central events. Second, the shape of the parton distribution functions implies there is likely to be more initial state radiation, since they are less steep in the large x region. Coupled with the fact that the large-rapidity jets are closer to the beams, it is interesting to see the dependence of jet mass on the jet rapidity.

Finally, the total transverse momentum in the event, H_T, is a measure of the activity of the event. Soft jets that are vetoed contribute to H_T and will affect the jet mass, but still fit into the same event selection criteria. The contribution of underlying event and pile-up will similarly affect the jet mass distribution, and H_T is a simple proxy for the size of these observables.

6.2.2. Jet shape measurements Jet shapes measure the radiation pattern within a jet by calculating a function of the momenta in the jet. The jet mass is a special jet shape, but there are other important jet shapes whose measurement would be very informative. We discuss several. Both N-subjettiness and planar flow are calculable, as they take moments of the momenta in the jet.

- N-subjettiness is a useful variable for jet substructure [38, 56]. N-subjettiness is defined with respect to a set of subjet axes q_i:

$$\tau_N^{(\beta)} = \frac{\sum_k p_{T,k} \left(\min\left\{\Delta R_{1,k}, \Delta R_{2,k}, \ldots, \Delta R_{N,k}\right\}\right)^\beta}{\sum_k p_{T,k}(R_0)^\beta}, \qquad (18)$$

where $\beta > 0$ is a real parameter, R_0 is the radius of the jet, and $\Delta R_{i,k}$ is the angular separation between particle k and subjet axis q_i. The shape $\tau_N^{(\beta)}$ probes how "N-subjet-like" a jet is, and provides an effective veto on additional subjets. Because adding more axes only lowers the value of $\tau_N^{(\beta)}$, N-subjettiness cannot provide a veto against fewer subjets.

The case $N = 1, \beta = 1$ is also known as girth, broadening, or width; $\beta = 2$ is related to the jet mass for small masses. These are the most common choices for β, and it would be interesting to compare them. Additionally, other choices of β can be informative, as they will probe the structure of the jet as a function of the angle to the 1-subjettiness axis. $\tau_1^{(\beta)}$ is similar to jet angularities, a jet shaped defined for e^+e^- events [53, 106, 98, 54]. The distribution in jet angularity τ_a was calculated to next-to-leading log accuracy in τ_a [54], and the theoretical tools exist to extend this calculation to the distribution of $\tau_1^{(\beta)}$ at the LHC.

2- and 3-subjettiness are also of interest. These can probe jets with multiple subjets, and the substructure of these jets will more closely resemble a boosted heavy object decay. (Using τ_3/τ_2 to identify top jets was studied in Section 5.)

- Planar flow is an interesting shape variable that was proposed to distinguish top and QCD jets [107, 75]. Planar flow is defined in terms of the eigenvalues of a 2-by-2 matrix, I_w, constructed from the components of momenta perpendicular to the jet axis:

$$I_w^{kl} = \frac{1}{m_J} \sum_{i \in J} \frac{p_i^{\perp k} p_i^{\perp l}}{E_i} \,, \tag{19}$$

where $p^{\perp k}$ is the kth component of p perpendicular to the jet axes (with respect to a pair of basis axes in the perpendicular plane). From I_w, planar flow is defined

$$Pf = \frac{4 \det I_w}{\text{tr}(I_w)^2} \,. \tag{20}$$

If the radiation in the jet is clustered along a line in the perpendicular plane going through the jet axis, then Pf will be close to 0. This will be the case for QCD jets and jets with 2-body kinematics, such as Higgs or W jets. For jets with 3-body (or more) kinematics, such as the top, Pf will be $\mathcal{O}(1)$.

- Subjet and track multiplicities have been shown to be effective discriminators of quark and gluon jets [45, 46]. Subjets can be found by reclustering the jet with a small radius, and finer resolution of the subjet size can improve discrimination between jets from different sources. The study of subjet multiplicity offers the chance to study the sensitivity to p_T or energy cutoffs placed on jet constituents or subjets. Does the energy resolution for subjets significantly improve with a higher energy cutoff on jet constituents? Does the multiplicity become sensitive to pile-up and the underlying event if the cutoff is taken too low? Similarly, the charged track multiplicity is a useful observable whose power depends on the angular resolution for track identification as well as the performance over the range of charged particle momenta in the jet.

6.2.3. Groomed jet measurements Many new physics searches can utilise jet grooming algorithms. Filtering, pruning, and trimming are jet grooming algorithms that modify the substructure of the jet to remove contributions from the underlying event and pile-up [35, 33, 34, 65]. These algorithms can be applied to a wide range of channels, and

comparing the performance of the three algorithms can instructive (cf. Section 6 of Ref. [1]). Because each algorithm operates on the substructure differently, it is useful to compare all of them. Experimental studies can quantify the performance of each algorithm and determine which is best for a given application.

Each grooming algorithm operates on a single jet and produces a groomed jet. Therefore any observable can be measured on the original jet and the groomed jet. The distributions before and after grooming are always of interest to understand the effects of grooming, and grooming algorithms can be used to study a variety of jet properties. The most interesting observables and objects to study with jet grooming are

- Jet mass.
- Pile-up and the underlying event are a large motivation for jet grooming methods. The performance with respect to pile-up for some jet grooming algorithms is currently being studied, and is quantified by studying tracks from secondary vertices. Quantifying the performance with respect to the underlying event is more challenging, but measures exist [101].
- If N-subjettiness is measured, then the effect of the grooming algorithms will be interesting to study. Grooming algorithms are designed to remove isolated soft radiation that can come from the underlying event or pile-up and contribute to poor mass resolution in the jet. This radiation will also have a large effect on N-subjettiness. Studying the N-subjettiness distribution (for $N = 1, 2, 3$) will give insight to grooming methods using an observable where it is simple to visualise jets with multiple energetic subjets.
- Given the good tracking and angular resolution at the LHC, the experiments can study the performance of grooming methods using only charged tracks.

6.2.4. Global event shapes Finally, event shapes are also of interest. While these are not direct jet substructure observables, they have a strong connection to jet substructure. Initial studies of jet substructure were driven by Monte Carlo studies, but more recently the theoretical foundations of jet substructure have been explored. Event shapes have traditionally been a testing ground for theoretical tools, and jet shapes are a by-product of these studies. N-subjettiness was built in analogy to N-jettiness, an event shape used to veto against additional jets in an event [50, 108, 109]. Like N-subjettiness, N-jettiness measures how $\leq N$-jet-like an event is. Measurements of event shapes can be compared directly to calculations, and the comparison is useful in building theoretical tools to calculate jet substructure properties. These observables are especially amenable to calculation, and in fact distributions of these observables have already been calculated in a variety of applications.

Observables of interest include:

- 0-jettiness, also known as beam thrust, is a measure of total hadronic activity away from the beams. In events without energetic jets, this can be used to study the underlying event and assist in tuning the Monte Carlo. In new physics searches

with a veto on any jets (e.g., $h \to WW$), the beam thrust distribution can be used to understand the theory uncertainties on the jet veto.

- 1-jettiness can be similarly implemented on events with a single jet, and can be used to veto against additional jets for an exclusive 1-jet sample. An ample background of $\gamma/W/Z+$ jet exists in which to study the 1-jettiness distribution.

- A number of event shapes have been proposed for study in dijet type events in [110] and examined in detail in [111], including observables related to thrust, broadening and jet rates (Y_{23}). Thrust-like observables show enhanced sensitivity to the underlying event, possibly allowing for powerful constraints on its properties, while Y_{23} provides a more direct sensitivity to perturbative effects. The distribution of Y_{23} has also been studied in [74]. The above observables have all been defined with particles as inputs. One can also study event shapes with jets as inputs and in one such study [112], Monte Carlos with matched matrix elements covering a range of jet multiplicities gave a worse description of event shape data than parton shower Monte Carlos (which only include $2 \to 2$ matrix elements matched directly onto the parton shower). This is troubling, and comparison to more event shapes can provide a way to differentiate different effects in the Monte Carlo simulations that may be contributing to this issue.

7. Concluding remarks

The field of jet substructure has made remarkable progress since its inception more than twenty years ago [113]. In this we report we have endeavoured to present a contemporary overview of jet substructure theory and practice. The experimental results published so far are encouraging and promising. They suggest that in the coming years jet substructure will play an important role in both Standard Model measurements and beyond-the-Standard-Model searches. New theoretical ideas for using and understanding jets continue to be developed. As substructure techniques proliferate, a unified understanding will be vital. The theoretical progress and goals discussed above are important steps along this path. Meanwhile, software tools like FastJet and SpartyJet provide a complementary method for understanding and exploring jet substructure techniques. We have given some examples of such exploration in this report, and we hope that the benchmark samples, tools, and comparisons we are making available will be useful tools in advancing jet substructure in 2012 and beyond.

References

[1] A. Abdesselam, E. Kuutmann, U. Bitenc, G. Brooijmans, J. Butterworth, *et al.*, "Boosted objects: A probe of beyond the Standard Model physics," *Eur.Phys.J.* **C71** (2011) 1661, arXiv:1012.5412 [hep-ph].

[2] **ATLAS** Collaboration, G. Aad *et al.*, "Study of jet shapes in inclusive jet production in pp collisions at $\sqrt{s} = 7$ TeV using the ATLAS detector," *Phys.Rev.* **D83** (2011) 052003, arXiv:1101.0070 [hep-ex].

[3] **CMS** Collaboration, "Jet transverse structure and momentum distribution in pp collisions at 7 TeV," Tech. Rep. CMS-PAS-QCD-10-014, CERN, Geneva, 2010.

[4] **ATLAS** Collaboration, "Measurement of jet mass and substructure for inclusive jets in $\sqrt{s} = 7$ TeV pp collisions with the ATLAS experiment," Tech. Rep. ATLAS-CONF-2011-073, CERN, Geneva, May, 2011.

[5] **CMS** Collaboration, "Study of jet substructure in pp collisions at 7 TeV in CMS," Tech. Rep. CMS-PAS-JME-10-013, CERN, 2010.

[6] M. Cacciari, G. P. Salam, and G. Soyez, "The catchment area of jets," *JHEP* **0804** (2008) 005, arXiv:0802.1188 [hep-ph].

[7] S. Sapeta and Q. C. Zhang, "The mass area of jets," *JHEP* **1106** (2011) 038, arXiv:1009.1143 [hep-ph].

[8] D. W. Miller, *Measurement of Hadronic Event Shapes and Jet Substructure in Proton-Proton Collisions at 7.0 TeV Center-of-Mass Energy with the ATLAS Detector at the Large Hadron Collider. CERN-THESIS-2011-144, SLAC-R-974*. PhD thesis, Stanford University, Menlo Park, CA, 2011. Presented 03 Jun 2011.

[9] **CDF** Collaboration, T. Aaltonen *et al.*, "The Substructure of High Transverse Momentum Jets Observed by CDF II," *CDF Note* **10199** (2010) .

[10] **CDF** Collaboration, T. Aaltonen *et al.*, "First search for multijet resonances in $\sqrt{s} = 1.96$ TeV $p\bar{p}$ collisions," *Phys.Rev.Lett.* **107** (2011) 042001, arXiv:1105.2815 [hep-ex].

[11] **CDF** Collaboration, "A search for boosted top quarks by CDF II," Tech. Rep. CDF/ANAL/TOP/PUBLIC/10234, Fermilab, June, 2011.

[12] A. Falkowski, J. T. Ruderman, T. Volansky, and J. Zupan, "Hidden Higgs decaying to lepton jets," *JHEP* **1005** (2010) 077, arXiv:1002.2952 [hep-ph].

[13] **D0** Collaboration, V. M. Abazov *et al.*, "Measurement of color flow in $t\bar{t}$ events from $p\bar{p}$ collisions at $\sqrt{s} = 1.96$ TeV," *Phys.Rev.* **D83** (2011) 092002, arXiv:1101.0648 [hep-ex].

[14] M. Dasgupta, L. Magnea, and G. P. Salam, "Non-perturbative QCD effects in jets at hadron colliders," *JHEP* **02** (2008) 055, arXiv:0712.3014 [hep-ph].

[15] S. D. Ellis, Z. Kunszt, and D. E. Soper, "Jets at hadron colliders at order α_s^3: A look inside," *Phys. Rev. Lett.* **69** (1992) 3615–3618, arXiv:hep-ph/9208249 [hep-ph].

[16] M. Cacciari, G. P. Salam, and G. Soyez, "The anti-kt jet clustering algorithm," *JHEP* **04** (2008) 063, arXiv:0802.1189 [hep-ph].

[17] W. Lampl, S. Laplace, D. Lelas, P. Loch, H. Ma, S. Menke, S. Rajagopalan, D. Rousseau,

S. Snyder, and G. Unal, "Calorimeter clustering algorithms: Description and performance," Tech. Rep. ATL-LARG-PUB-2008-002 and ATL-COM-LARG-2008-003, CERN, Geneva, Apr, 2008.

[18] **CDF** Collaboration, T. Aaltonen *et al.*, "Search for new particles decaying into dijets in proton- antiproton collisions at $\sqrt{s} = 1.96$ TeV," *Phys. Rev.* **D79** (2009) 112002, `arXiv:0812.4036 [hep-ex]`.

[19] **CDF** Collaboration, F. Abe *et al.*, "A Measurement of jet shapes in $p\bar{p}$ collisions at $\sqrt{s} = 1.8$ TeV," *Phys.Rev.Lett.* **70** (1993) 713–717.

[20] **D0** Collaboration, S. Abachi *et al.*, "Transverse energy distributions within jets in $p\bar{p}$ collisions at $\sqrt{s} = 1.8$ TeV," *Phys.Lett.* **B357** (1995) 500–508.

[21] **ZEUS** Collaboration, S. Chekanov *et al.*, "Substructure dependence of jet cross sections at HERA and determination of α_s," *Nucl. Phys. B* **700** (2004) 3.

[22] **ZEUS** Collaboration, J. Breitweg *et al.*, "Measurement of jet shapes in high Q^2 deep inelastic scattering at HERA," *Eur.Phys.J.* **C8** (1999) 367–380, `arXiv:hep-ex/9804001 [hep-ex]`.

[23] **H1** Collaboration, C. Adloff *et al.*, "Measurement of internal jet structure in dijet production in deep inelastic scattering at HERA," *Nucl.Phys.* **B545** (1999) 3–20, `arXiv:hep-ex/9901010 [hep-ex]`.

[24] **ZEUS** Collaboration, J. Breitweg *et al.*, "Measurement of jet shapes in photoproduction at HERA," *Eur.Phys.J.* **C2** (1998) 61–75, `arXiv:hep-ex/9710002 [hep-ex]`.

[25] **OPAL** Collaboration, R. Akers *et al.*, "QCD studies using a cone based jet finding algorithm for e^+e^- collisions at LEP," *Z.Phys.* **C63** (1994) 197–212.

[26] **OPAL** Collaboration, K. Ackerstaff *et al.*, "Multiplicity distributions of gluon and quark jets and tests of QCD analytic predictions," *Eur.Phys.J.* **C1** (1998) 479–494, `arXiv:hep-ex/9708029 [hep-ex]`.

[27] **ATLAS** Collaboration, "Jet shapes in ATLAS and MC modeling," Tech. Rep. ATL-PHYS-PUB-2011-010, CERN, Geneva, Jul, 2011.

[28] **ATLAS** Collaboration, "New ATLAS event generator tunes to 2010 data," Tech. Rep. ATL-PHYS-PUB-2011-008, CERN, Geneva, Apr, 2011.

[29] **ATLAS** Collaboration, "A search for new high-mass phenomena producing top quarks with the ATLAS experiment," Tech. Rep. ATLAS-CONF-2011-070, CERN, Geneva, May, 2011.

[30] **CMS** Collaboration, "The Jet Plus Tracks algorithm for calorimeter jet energy corrections in CMS," Tech. Rep. CMS-PAS-JME-09-002, CERN, Geneva, 2009.

[31] D. E. Kaplan, K. Rehermann, M. D. Schwartz, and B. Tweedie, "Top tagging: A method for identifying boosted hadronically decaying top quarks," *Phys. Rev. Lett.* **101** (2008) 142001, `arXiv:0806.0848 [hep-ph]`.

[32] S. Rappoccio, "A new top jet tagging algorithm for highly boosted top jets," Tech. Rep. CMS-CR-2009-255, CERN, Geneva, Aug, 2009.

[33] S. D. Ellis, C. K. Vermilion, and J. R. Walsh, "Techniques for improved heavy particle searches with jet substructure," *Phys. Rev.* **D80** (2009) 051501, `arXiv:0903.5081 [hep-ph]`.

[34] S. D. Ellis, C. K. Vermilion, and J. R. Walsh, "Recombination algorithms and jet substructure: Pruning as a tool for heavy particle searches," *Phys. Rev.* **D81** (2010) 094023, `arXiv:0912.0033 [hep-ph]`.

[35] J. M. Butterworth, A. R. Davison, M. Rubin, and G. P. Salam, "Jet substructure as a new Higgs search channel at the LHC," *Phys. Rev. Lett.* **100** (2008) 242001, `arXiv:0802.2470 [hep-ph]`.

[36] **CMS** Collaboration, "Search for BSM $t\bar{t}$ production in the boosted all-hadronic final state," Tech. Rep. CMS-PAS-EXO-11-006, CERN, 2011.

[37] T. Plehn and M. Spannowsky, "Top tagging," `arXiv:1112.4441 [hep-ph]`.

[38] J. Thaler and K. Van Tilburg, "Identifying boosted objects with N-subjettiness," *JHEP* **03** (2011) 015, `arXiv:1011.2268 [hep-ph]`.

[39] J.-H. Kim, "Rest frame subjet algorithm with SISCone jet for fully hadronic decaying Higgs

search," *Phys.Rev.* **D83** (2011) 011502, `arXiv:1011.1493 [hep-ph]`.

[40] A. Hook, M. Jankowiak, and J. G. Wacker, "Jet dipolarity: Top tagging with color flow," `arXiv:1102.1012 [hep-ph]`.

[41] M. Jankowiak and A. J. Larkoski, "Jet substructure without trees," *JHEP* **1106** (2011) 057, `arXiv:1104.1646 [hep-ph]`.

[42] L. G. Almeida, S. J. Lee, G. Perez, G. Sterman, and I. Sung, "Template overlap method for massive jets," *Phys.Rev.* **D82** (2010) 054034, `arXiv:1006.2035 [hep-ph]`.

[43] D. E. Soper and M. Spannowsky, "Finding physics signals with shower deconstruction," *Phys.Rev.* **D84** (2011) 074002, `arXiv:1102.3480 [hep-ph]`.

[44] T. Plehn, G. P. Salam, and M. Spannowsky, "Fat jets for a light Higgs," *Phys. Rev. Lett.* **104** (2010) 111801, `arXiv:0910.5472 [hep-ph]`.

[45] J. Gallicchio and M. D. Schwartz, "Quark and gluon tagging at the LHC," *Phys.Rev.Lett.* **107** (2011) 172001, `arXiv:1106.3076 [hep-ph]`.

[46] J. Gallicchio and M. D. Schwartz, "Pure samples of quark and gluon jets at the LHC," *JHEP* **1110** (2011) 103, `arXiv:1104.1175 [hep-ph]`.

[47] D. Krohn, L. Randall, and L.-T. Wang, "On the feasibility and utility of ISR tagging," `arXiv:1101.0810 [hep-ph]`.

[48] G. D. Kribs, A. Martin, T. S. Roy, and M. Spannowsky, "Discovering the Higgs Boson in New Physics Events using Jet Substructure," *Phys. Rev.* **D81** (2010) 111501, `arXiv:0912.4731 [hep-ph]`.

[49] G. D. Kribs, A. Martin, T. S. Roy, and M. Spannowsky, "Discovering Higgs bosons of the MSSM using jet substructure," *Phys.Rev.* **D82** (2010) 095012, `arXiv:1006.1656 [hep-ph]`.

[50] I. W. Stewart, F. J. Tackmann, and W. J. Waalewijn, "N-Jettiness: An inclusive event shape to veto jets," *Phys. Rev. Lett.* **105** (2010) 092002, `arXiv:1004.2489 [hep-ph]`.

[51] S. Catani, Y. L. Dokshitzer, M. H. Seymour, and B. R. Webber, "Longitudinally invariant K(t) clustering algorithms for hadron hadron collisions," *Nucl. Phys.* **B406** (1993) 187–224.

[52] S. D. Ellis and D. E. Soper, "Successive combination jet algorithm for hadron collisions," *Phys. Rev.* **D48** (1993) 3160–3166, `arXiv:hep-ph/9305266`.

[53] C. F. Berger, T. Kucs, and G. F. Sterman, "Event shape / energy flow correlations," *Phys. Rev.* **D68** (2003) 014012, `arXiv:hep-ph/0303051`.

[54] S. D. Ellis, A. Hornig, C. Lee, C. K. Vermilion, and J. R. Walsh, "Jet shapes and jet algorithms in SCET," *JHEP* **11** (2010) 101, `arXiv:1001.0014 [hep-ph]`.

[55] S. Catani, G. Turnock, and B. R. Webber, "Jet broadening measures in e^+e^- annihilation," *Phys. Lett.* **B295** (1992) 269–276.

[56] J. Thaler and K. Van Tilburg, "Maximizing boosted top identification by minimizing N-subjettiness," *JHEP* **1202** (2012) 093, `arXiv:1108.2701 [hep-ph]`.

[57] S. P. Lloyd, "Least squares quantization in pcm," *IEEE Transactions on Information Theory* **28** (1982) 129–137.

[58] J. Gallicchio and M. D. Schwartz, "Seeing in color: Jet superstructure," *Phys. Rev. Lett.* **105** (2010) 022001, `arXiv:1001.5027 [hep-ph]`.

[59] M. Jankowiak and A. J. Larkoski, "Angular scaling in jets,," `arXiv:1201.2688 [hep-ph]`.

[60] T. Plehn, M. Spannowsky, M. Takeuchi, and D. Zerwas, "Stop reconstruction with tagged tops," *JHEP* **1010** (2010) 078, `arXiv:1006.2833 [hep-ph]`.

[61] T. Plehn, M. Spannowsky, and M. Takeuchi, "Boosted semileptonic tops in stop decays," *JHEP* **1105** (2011) 135, `arXiv:1102.0557 [hep-ph]`.

[62] T. Plehn, M. Spannowsky, and M. Takeuchi, "How to improve top tagging," *Phys.Rev.* **D85** (2012) 034029, `arXiv:1111.5034 [hep-ph]`.

[63] **ATLAS** Collaboration, "Light-quark and gluon jets in ATLAS," Tech. Rep. ATLAS-CONF-2011-053, CERN, Geneva, Apr, 2011.

[64] M. Perelstein, M. E. Peskin, and A. Pierce, "Top quarks and electroweak symmetry breaking in little Higgs models," *Phys.Rev.* **D69** (2004) 075002, `arXiv:hep-ph/0310039 [hep-ph]`.

[65] D. Krohn, J. Thaler, and L.-T. Wang, "Jet trimming," *JHEP* **1002** (2010) 084, `arXiv:0912.1342 [hep-ph]`.

[66] M. Cacciari, G. P. Salam, and G. Soyez. `http://fastjet.fr`.

[67] Y. Cui, Z. Han, and M. D. Schwartz, "*W*-jet tagging: Optimizing the identification of boosted hadronically-decaying *W* bosons," *Phys.Rev.* **D83** (2011) 074023, `arXiv:1012.2077 [hep-ph]`.

[68] T. Gleisberg, S. Hoeche, F. Krauss, A. Schalicke, S. Schumann, *et al.*, "SHERPA 1.alpha: A proof of concept version," *JHEP* **0402** (2004) 056, `arXiv:hep-ph/0311263 [hep-ph]`.

[69] T. Gleisberg, S. Hoeche, F. Krauss, M. Schonherr, S. Schumann, *et al.*, "Event generation with SHERPA 1.1," *JHEP* **0902** (2009) 007, `arXiv:0811.4622 [hep-ph]`.

[70] S. Hoeche, F. Krauss, S. Schumann, and F. Siegert, "QCD matrix elements and truncated showers," *JHEP* **0905** (2009) 053, `arXiv:0903.1219 [hep-ph]`.

[71] S. Hoeche, S. Schumann, and F. Siegert, "Hard photon production and matrix-element parton-shower merging," *Phys.Rev.* **D81** (2010) 034026, `arXiv:0912.3501 [hep-ph]`.

[72] T. Gleisberg and S. Hoeche, "Comix, a new matrix element generator," *JHEP* **0812** (2008) 039, `arXiv:0808.3674 [hep-ph]`.

[73] S. Schumann and F. Krauss, "A parton shower algorithm based on Catani-Seymour dipole factorisation," *JHEP* **0803** (2008) 038, `arXiv:0709.1027 [hep-ph]`.

[74] **ATLAS** Collaboration, G. Brooijmans, "High pt hadronic top quark identification part 1 : Jet mass and ysplitter," Tech. Rep. ATL-PHYS-CONF-2008-008, CERN, Geneva, 2008.

[75] J. Thaler and L.-T. Wang, "Strategies to identify boosted tops," *JHEP* **07** (2008) 092, `arXiv:0806.0023 [hep-ph]`.

[76] A. Hoecker, P. Speckmayer, J. Stelzer, J. Therhaag, E. von Toerne, and H. Voss, "TMVA toolkit for multivariate data analysis with ROOT," 2010. `http://tmva.sourceforge.net`.

[77] P.-A. Delsart, K. L. Geerlings, J. Huston, B. T. Martin, and C. K. Vermilion, "SpartyJet 4.0 user's manual," `arXiv:1201.3617 [hep-ex]`.

[78] P.-A. Delsart, K. L. Geerlings, J. Huston, B. T. Martin, and C. K. Vermilion. `http://projects.hepforge.org/spartyjet`.

[79] M. Cacciari and G. P. Salam, "Dispelling the N^3 myth for the k_t jet-finder," *Phys. Lett.* **B641** (2006) 57–61, `arXiv:hep-ph/0512210`.

[80] C. W. Bauer, S. Fleming, and M. E. Luke, "Summing Sudakov logarithms in $B \to X_s \gamma$ in effective field theory," *Phys. Rev.* **D63** (2000) 014006, `arXiv:hep-ph/0005275`.

[81] C. W. Bauer, S. Fleming, D. Pirjol, and I. W. Stewart, "An effective field theory for collinear and soft gluons: Heavy to light decays," *Phys. Rev.* **D63** (2001) 114020, `arXiv:hep-ph/0011336`.

[82] C. W. Bauer and I. W. Stewart, "Invariant operators in collinear effective theory," *Phys. Lett.* **B516** (2001) 134–142, `arXiv:hep-ph/0107001`.

[83] C. W. Bauer, D. Pirjol, and I. W. Stewart, "Soft-collinear factorization in effective field theory," *Phys. Rev.* **D65** (2002) 054022, `arXiv:hep-ph/0109045`.

[84] C. W. Bauer, S. P. Fleming, C. Lee, and G. F. Sterman, "Factorization of e^+e^- event shape distributions with hadronic final states in soft collinear effective theory," *Phys. Rev.* **D78** (2008) 034027, `arXiv:0801.4569 [hep-ph]`.

[85] C. W. Bauer, A. Hornig, and F. J. Tackmann, "Factorization for generic jet production," *Phys. Rev.* **D79** (2009) 114013, `arXiv:0808.2191 [hep-ph]`.

[86] J. R. Walsh and S. Zuberi, "Factorization constraints on jet substructure," `arXiv:1110.5333 [hep-ph]`.

[87] I. W. Stewart, F. J. Tackmann, and W. J. Waalewijn, "Factorization at the LHC: From PDFs to initial state jets," *Phys. Rev.* **D81** (2010) 094035, `arXiv:0910.0467 [hep-ph]`.

[88] A. Banfi and M. Dasgupta, "Problems in resumming interjet energy flows with k_t clustering," *Phys.Lett.* **B628** (2005) 49–56, `arXiv:hep-ph/0508159 [hep-ph]`.

[89] Y. Delenda, R. Appleby, M. Dasgupta, and A. Banfi, "On QCD resummation with k(t)

clustering," *JHEP* **0612** (2006) 044, `arXiv:hep-ph/0610242 [hep-ph]`.

[90] M. Dasgupta and G. Salam, "Resummation of nonglobal QCD observables," *Phys.Lett.* **B512** (2001) 323–330, `arXiv:hep-ph/0104277 [hep-ph]`.

[91] R. Appleby and M. Seymour, "Nonglobal logarithms in interjet energy flow with kt clustering requirement," *JHEP* **0212** (2002) 063, `arXiv:hep-ph/0211426 [hep-ph]`.

[92] A. Banfi, G. Marchesini, and G. Smye, "Away-from-jet energy flow," *JHEP* **08** (2002) 006, `arXiv:hep-ph/0206076`.

[93] A. Banfi, M. Dasgupta, K. Khelifa-Kerfa, and S. Marzani, "Non-global logarithms and jet algorithms in high-pT jet shapes," *JHEP* **1008** (2010) 064, `arXiv:1004.3483 [hep-ph]`.

[94] R. Kelley, M. D. Schwartz, R. M. Schabinger, and H. X. Zhu, "The two-loop hemisphere soft function," *Phys.Rev.* **D84** (2011) 045022, `arXiv:1105.3676 [hep-ph]`.

[95] A. Hornig, C. Lee, I. W. Stewart, J. R. Walsh, and S. Zuberi, "Non-global structure of the $O(\alpha_s^2)$ dijet soft function," *JHEP* **08** (2011) 054, `arXiv:1105.4628 [hep-ph]`.

[96] A. Hornig, C. Lee, J. R. Walsh, and S. Zuberi, "Double non-global logarithms In-N-Out of jets," *JHEP* **1201** (2012) 149, `arXiv:1110.0004 [hep-ph]`.

[97] M. Dasgupta and G. P. Salam, "Resummed event shape variables in DIS," *JHEP* **0208** (2002) 032, `arXiv:hep-ph/0208073 [hep-ph]`.

[98] S. D. Ellis, A. Hornig, C. Lee, C. K. Vermilion, and J. R. Walsh, "Consistent factorization of jet observables in exclusive multijet cross-sections," *Phys. Lett.* **B689** (2010) 82–89, `arXiv:0912.0262 [hep-ph]`.

[99] C. W. Bauer, F. J. Tackmann, J. R. Walsh, and S. Zuberi, "Factorization and Resummation for Dijet Invariant Mass Spectra," `arXiv:1106.6047 [hep-ph]`.

[100] M. Cacciari, M. Dasgupta, L. Magnea, and G. Salam, "Power corrections for jets at hadron colliders," `arXiv:0706.3157 [hep-ph]`.

[101] M. Cacciari, G. P. Salam, and S. Sapeta, "On the characterisation of the underlying event," *JHEP* **04** (2010) 065, `arXiv:0912.4926 [hep-ph]`.

[102] C. Lee and G. F. Sterman, "Universality of nonperturbative effects in event shapes," *eConf* **C0601121** (2006) A001, `arXiv:hep-ph/0603066 [hep-ph]`.

[103] C. Lee and G. F. Sterman, "Momentum flow correlations from event shapes: Factorized soft gluons and soft-collinear effective theory," *Phys. Rev.* **D75** (2007) 014022, `arXiv:hep-ph/0611061`.

[104] A. H. Hoang and I. W. Stewart, "Designing gapped soft functions for jet production," *Phys. Lett.* **B660** (2008) 483–493, `arXiv:0709.3519 [hep-ph]`.

[105] **CDF** Collaboration, T. Aaltonen *et al.*, "Study of substructure of high transverse momentum jets produced in proton-antiproton collisions at $\sqrt{s} = 1.96$ TeV," `arXiv:1106.5952 [hep-ex]`.

[106] A. Hornig, C. Lee, and G. Ovanesyan, "Effective Predictions of Event Shapes: Factorized, Resummed, and Gapped Angularity Distributions," *JHEP* **05** (2009) 122, `arXiv:0901.3780 [hep-ph]`.

[107] L. G. Almeida *et al.*, "Substructure of high-p_T Jets at the LHC," *Phys. Rev.* **D79** (2009) 074017, `arXiv:0807.0234 [hep-ph]`.

[108] C. F. Berger, C. Marcantonini, I. W. Stewart, F. J. Tackmann, and W. J. Waalewijn, "Higgs production with a central jet veto at NNLL+NNLO," *JHEP* **04** (2011) 092, `arXiv:1012.4480 [hep-ph]`.

[109] T. T. Jouttenus, I. W. Stewart, F. J. Tackmann, and W. J. Waalewijn, "The soft function for exclusive N-jet production at hadron colliders," *Phys. Rev.* **D83** (2011) 114030, `arXiv:1102.4344 [hep-ph]`.

[110] A. Banfi, G. P. Salam, and G. Zanderighi, "Resummed event shapes at hadron - hadron colliders," *JHEP* **0408** (2004) 062, `arXiv:hep-ph/0407287 [hep-ph]`. Erratum added online, nov/29/2004.

[111] A. Banfi, G. P. Salam, and G. Zanderighi, "Phenomenology of event shapes at hadron

colliders," *JHEP* **1006** (2010) 038, `arXiv:1001.4082 [hep-ph]`.

[112] **CMS** Collaboration, V. Khachatryan *et al.*, "First measurement of hadronic event shapes in *pp* collisions at $\sqrt{s} = 7$ TeV," *Phys. Lett.* **B699** (2011) 48–67, `arXiv:1102.0068 [hep-ex]`.

[113] M. Seymour, "Tagging a heavy Higgs boson," in *Proceedings of the ECFA LHC Workshop (Aachen, Germany, 4–9 October 1990)*, vol. 2, pp. 557–569. 1990.